1-18-2022

ALGORITHMS FOR RAPID TRIP DETECTION IN HUMAN WALKING USING INERTIAL SENSORS

Chadi Ellouzi
Rowan University

ALGORITHMS FOR RAPID TRIP DETECTION IN HUMAN WALKING USING INERTIAL SENSORS

by

Chadi Ellouzi

A Thesis

Submitted to the
Department of Mechanical Engineering
Henry M. Rowan College of Engineering
In partial fulfillment of the requirement
For the degree of
Master of Science in Mechanical Engineering
at
Rowan University
December 20th 2021

Thesis Chair: Mitja Trkov, Ph.D.

Committee Members:
Behrad Koohbor, Ph.D.
Chen Shen, Ph.D.

Dedications

I would like to dedicate this manuscript to my family, whose unconditional love and support has made this possible. I would like to thank my parents, for always pushing me to be better, even beyond what I thought was possible. I would also like to thank my friends, for supporting me when I needed it most and always acting more mature than me. Thank you all, as I wouldn’t be at this position without your support.

Acknowledgements

I would like to express my gratitude to my advisor and mentor, Dr. Mitja Trkov. Your constant guidance and support over the past two years has made me a better researcher and engineer. Working in your lab has been a wonderful experience, the knowledge I have gained and the work I have accomplished with your guidance is proving to be invaluable.

I would also like to thank Dr. Shen, for his support and understanding through the process of obtaining my research objectives. Further, I would like to thank Dr. Ratneshwar Jha, Dr. Francis Haas and all the people that contributed directly or indirectly to my support and growth and for their support throughout my time at the mechanical engineering Department and Rowan University.

I would like to extend a thank you to my friends, lab mates for their expertise which aided in my research, and the memories we shared over the past two years and for the laughs and experiences we shared.

Abstract

Chadi Ellouzi
ALGORITHMS FOR RAPID TRIP DETECTION IN HUMAN WALKING USING INERTIAL SENSORS
2021-2022
Mitja Trkov, Ph.D.
Master of Science in Mechanical Engineering

Trips and falls are one of the most common causes for injuries among elderly. The existing trip-and-falls studies primarily focus on the proactive fall prevention approaches, while active prevention strategies remain largely unexplored. This thesis aims to provide first steps towards active trip-and-fall prevention by developing various algorithms capable of detecting trip in human walking faster than the human voluntary reactions (~200 ms). The measurements of human kinematics are used as the inputs in the algorithms. The proposed algorithms include three threshold-based detection methods, an optimized elastic time-series alignment tool called dynamic time warping (DTW) that overcomes problems of time dependency and signal phasing, and an optimized signal-frequency decomposition method known as continuous wavelet transform (CWT) that allows signal analysis in time-frequency domain. In addition, a planar covariation law (PCL), which is an intersegmental co-ordination kinematic law that relates lower limb angles during walking, is explored for trip gaits for the first time. A quantification of trip perturbation as a function of perturbation duration was developed to provide an insight about trip evolution and severity. The developed rapid trip detection algorithms integrated and combined with assistive technologies have the potential to serve as an enabling tools of future trip-and-fall prevention strategies.

Table of Contents

Table of Contents (Continued)

Table of Contents (Continued)

List of Figures

Figure Page

List of Figures (Continued)

Figure Page

List of Figures (Continued)

Figure Page

List of Figures (Continued)

Figure Page

Chapter 1

Introduction

1.1. Introduction to Human Gait Perturbations

1.1.1. *Background Information*

Unforeseen gait perturbations (i.e., trips and slips) during locomotion are the main culprits of falls in elderly population. Trips and slips lead to a loss of balance and effect the stability of gait and they are associated with up to 53% of falls in such communities [1-3]. However, researchers have shown that individuals begin to have an increased relative risk of falls long before retirement age due to the start of slower reflexes and the non-ability to react effectively compared to their young counterpart [4-5].

The consequences of falls, combined with improper recovery techniques often lead to variety of injuries and are associated with approximately 11% of serious injuries in elderly population and have a direct impact on the expansion of the healthcare services costs [6-8]. Studies of patients attending emergency departments have shown that gait perturbation accidents caused 55.4% of the total fractures occurred for men and 75.9% of total fractures for the women [9]. A random survey of patients that suffered bone fractures and required surgical operation showed that 50% of those patients had some kind of disability one year after an injury [9]. Moreover, the gait perturbation phenomena's result in tens of thousands of "minor" injuries such as sprains, strains, contusions and lacerations each year [10]. Thus, in order minimize fall-related economic costs it is important to advance the understanding about trip occurrences and fall

prevention strategies. Many biomechanical studies have investigated the trip and fall phenomena examining the influencing factors causing trip and post-trip human balance recovery strategies [11]. In general, multiple factors contribute to the selection of recovery strategies. In the literature, the convention about the recovery strategies selected by the person is often associated with the timing of the trip onset during walking gait (i.e., the swing phase), despite the fact that the swing percentage is not a physical quantity that can be directly measured and an existing large variability in employed recovery strategies by subjects during mid-swing (40-70%) gait [12].

Three most commonly observed trip-induced recovery strategies include (i) the lowering strategy when trip happens during the late swing phase, (ii) the elevating strategy for trip onset in early swing perturbation, and (iii) the reaching strategy if trip occurs in the late swing gate phase [13-16]. Recently, model-based prediction of employed strategies was developed, however, for the purpose of this study and specific focus on trip detection, a convention based on swing percentage was used. Studies that investigated the effect of walking speed on the trip onset and recovery outcome reported opposite effects. In [17], slow walking speed was shown to be associated with a higher risk for trips, especially in the elderly population. However, a study in [18], suggested that fast walking speed helped subjects to successfully recover from the trip as opposite to what would be expected. Furthermore, later study [19] showed that the human response (reaction) time is more important for successful trip recovery strategy compared to the walking speed and that the duration of body forward rotation after a trip can affect the recovery capabilities.

Other studies on trip induced falls confirmed that there exists a critical point of body orientation with respect to the center of body mass during the trip, beyond which it is hard to initiate a successful recovery [20].Moreover, studies investigating the direction of a fall and the likely impact location of the human body for different types of trip-induced falls at various gait speeds (i.e., 1.99m/s, 1.43m/s and 0.66m/s) revealed that trips always resulted in a forward fall with frontal impacts into abdominal pelvis location regardless of the gait speed or when the trip was induced [21].

Current methodologies for trip-and-fall prevention rely on preventative approaches by improving subjects' trip balance recovery reactions through exposing subjects to repetitive trip exposure training [12]. Such training helps improve the trip balance recovery of the subjects by an increased margin of stability and step length during recovery steps [12]. For the purpose of active trip prevention using robotic interventions, a rapid trip detection is required as a first step. Many previous studies focused on trip-and-fall detection devices and algorithms [22-25].

Unfortunately, all these systems and algorithms are not efficient enough to be used for rapid trip-and-fall detection due to their slow algorithm processing time to detect the perturbation and their high false alarm rates. Based on the authors' best knowledge there does not exist any active system that can directly detect trips and assist with balance recovery to prevent trip-and-fall in real-time applications. Due to the rapid nature of trip perturbation, such a system would require fast trip detection (<100 ms) and an external assistance by the assistive device. This is required to allow sufficient time for the device

to provide active assistance by exerting an assistive torque to perform corrective balance recovery.

1.1.2. *Trip and Fall Definitions*

Trip is typically defined as the sudden stop of the swing foot movement while the individual's momentum makes the body center of mass shift forward leading to a balance loss that can result in a fall [20].

Figure 1

Comparison Between Trip and Normal Walking Gait

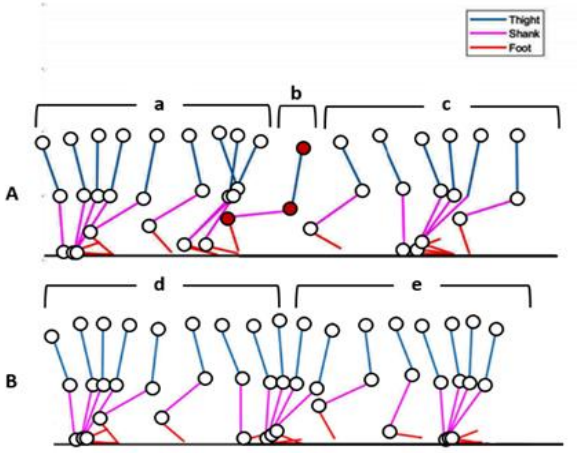

Note. Trip event versus normal walking is presented using stick figure presentation. White circles present hip, knee, and ankle joints, respectively. Blue segment presents thigh, magenta presents shank and red presents the foot of the participant. A, walking with trip event induced. a, Stance phase. b, Trip onset. c, Recovery phase. B, Normal walking without trip. d, Stance and swing phase. e, Heel to heel strike.

Trips typically happen due to the unevenness of a surface or an obstructed view. Figure 1 shows a stick figure comparison of a swing foot trajectory for trip and normal walking gait.

A fall is defined as the body's fast downward movement without any control of the rate neither the angle of that movement, from a higher to a lower level [26]. Falls due to trips are characterized by a shift of the body center of mass forward and an increase in the body angular acceleration to an irreversible point at which upright balance is lost.

1.2. Gait Perturbation Detection Systems

1.2.1. *Individual Wearable Systems*

Gait perturbations like slips and trip may result in the variation of key biomechanical parameters of the human body, which provide important indicators to detect those phenomena. For such purpose, individual wearable systems that allow to measure those quantities can be used to detect gait perturbations. Previous studies on fall and gait perturbation detections often used accelerometers, gyroscopes, and electrocardiography (ECG) as primary systems in their data collection [27-29], while others used glucometers, pressure sensors, electroencephalography (EEG) or electromyography (EMG) [30-31].

The choice of which system can be used depend on the overall purpose, performance requirements, desired results, and practicality of using the system in specific environments. Overall, the small, wearable systems provide an advantage compared to a larger stationary system to be used for such purposes due to their light weight, and the

ability to be used in an everyday environment during activities of daily living as compared to other laboratory-based systems.

1.2.2. *Visual Wearable Systems*

Vision-based fall detection systems has gained popularity in recent years, due to not requiring subjects to wear any sensors or devices. Extensive research in this direction has been demonstrated, and some of which [32-33] show promising performance and results. Although most of the visual systems are mainly in forms of cameras and are not light weight, cheap, and portable as wearable devices, they offer advantages which make them a good candidate depending upon the environment that they going to be used at and required system performance.

Most fixed RGB cameras are not intrusive and can operate wirelessly which eliminate the constraints of battery life encountered in the wearable devices' categories. Studies that used vision-based approach systems have used infrared cameras [34], RGB cameras [35], and RGB-D depth cameras [36]. However, their use is limited to indoor spaces and prone to occlusions, therefore limiting their applicability for everyday use and outdoor environment.

1.2.3. *Ambient Systems*

Ambient sensor-based detection systems have been developed in recent years that use variables from the ambient sensor as inputs. Studies conducted on fall and gait perturbation detection that used ambient sensors as their primary data collection and detection systems used active infrared, magnetic switches, and ultrasonic system [37-38],

while others used microphones and vibration sensors [39-40]. The selection of the appropriate tool to be used for the detection purposes depends on many factors such as cost and environmental conditions.

The ambient-based systems are an alternative option, since they are non-intrusive systems which provide more flexibility and comfort compared to other detection systems which can be more heavy or complex to operate. However, these systems introduce complexity in measurements and suffer from sensitivity issues, as they cannot operate in diverse environmental conditions such as high humidity or temperature.

1.3. Detection Time and Sensors Quantifications for Different Trip Detection Systems

1.3.1. *Pre-Impact Leading Detection Time*

Pre-impact leading detection time is defined as the elapsed time from fall detection to body-ground impact and it provides information about how fast and efficient the fall detection system is. Many studies reported the pre-impact leading detection time using different algorithms and systems with the longest reported time being 750 ms, the shortest being 150 ms, and an average of 450 ms [41-42].

For the purpose of trip detection, the desired pre-impact detection time should be as long as possible, as this means that the algorithm can detect trip sooner, ideally immediately after its onset. Moreover, this also allows more time to assist human perform any recovery strategy to prevent a fall.

1.3.2. *Trip Detection Time*

The trip detection time is different than the more commonly reported pre-impact leading detection time in the fall detection literature. The trip detection time is defined as time elapsed from trip onset to trip detection and it provides information about how efficient and fast the detection system is. Short detection time can significantly impact the real-time implementation by allowing additional time to provide external assistance by robotic devices. Many studies reported a wide range of trip detection times [43-45], with the fastest reported detection time being 359 ms [46].

1.3.3. *Sensors Number*

Number of sensors used in trip detection systems plays a significant role affecting accuracy and complexity of the system. An increased number of sensors allows to measure and record additional kinematic data resulting in a higher accuracy of the algorithm, however, it results in higher cost and complexity of the system. Most studies on fall and gait perturbation detection used one or two individual wearables inertial sensors attached to a different location on the human body [47-50], while some studies investigated use of up to four sensors depending on the experimental setup and desired result [51-52].

1.3.4. *Sensors Locations*

The inertial sensor locations are chosen based on the desired kinematic parameters to be recorded and analyzed. Most studies focusing on trip and fall detection used lower back and chest as primary location for their inertial sensors, since the motion

of the trunk was shown to be a good indicator of a fall event [53-55]. Studies investigating more diverse location for the sensor's placement included upper back, hips, and head locations, to provide indication about trip onset based on the measurements of the angular momentum observed during fall events [56-59].

1.4. Gait Perturbation Detection Systems in Biomedical Applications

Gait perturbation detection algorithms have been extensively researched due to its importance and utility and had a wide range of application in biomedical field. Some algorithms use static thresholds approach based on some kinematic parameters in order to detect falls [60-61], while others use an adaptive dynamic one for better efficiency [62-63]. Other studies used different approach and used machine learning and virtual reality in order to detect fall [64-65].

Pre-impact fall wearable detection systems have been proposed to be an effective fall prevention strategy and many of those systems have been commercialized in the market (i.e., MedicalGardien, MobileHelp). is still not fully explored and the algorithms of trip detection are still in their preliminary phase. Providing a rapid trip detection algorithm can be a valuable resource as part of the implementing an active trip-and-fall prevention strategy using robotic assistive device, since it is a required part that has to be integrated in the device design and embedded in the control algorithm of device.

Rapid trip detection is required to provide sufficient time for the device to provide active external assistance during the trip recovery to prevent falls and injuries. The main focus of this study is to provide a variety of algorithm in both time domain and frequency

domain based on fixed threshold methods in order to detect trip effectively and in a time shorter that the human reflexes, which is approximately 200 ms.

The first chapter of this work aims to provide an adequate literature review about the gait perturbation detection and the previous findings related to this topic in addition to different experimental tools used to provide an algorithm capable of trip detection. The second chapter aims to provide different technical aspects of the experimental setup used in this work, including platforms instrumentations and research protocol. In Chapter 3, two-time domain trip detection algorithms approaches using fixed threshold and elastic signal alignment method based on the lower back angular acceleration are discussed and the different results obtained by such algorithm are shown.

In Chapter 4, a frequency domain detection algorithm based on a continuous wavelet transform technique was used in the first part in order to provide a new manner to detect signals anomalies in frequency domain. In the second part, a qualitative approach was used based on a planar correlation law (PCL) that connects different lower joint kinematics through a planar relationship in order to provide a descriptive approach for trip detection and gait perturbation in general. Finally, a conclusion that provides a comparative approach was introduced in order to provide an overall picture of different algorithms used in this work in addition to the efficiency of each one of them as with respect to the other. Such work aims to expose new methods and techniques that can be used not only to detect trip in the biomechanical filed but also in related fields were signal anomalies need to be detected and quantified respectively.

Chapter 2

Trip Platform Design, Experimental Protocol and Data Acquisition System

In this chapter, the design process and requirements of the mechanical platform used to induce trips are presented. The experimental protocol for human subject testing, the data acquisition systems for data collection, and the pre- and post-processing signal analysis and procedures are discussed. The overall goal of this chapter is to present the experimental setup and protocols used to perform human subject experiments and measure human kinematics during human regular walking with trip perturbation on a flat surface. The data post-processing procedures described in this chapter are used to investigate the human reactions to trips and analyze the kinematics data of subjects' body motion responses to the trip onset. Careful design of experiments and high-quality data collection are important to guarantee the integrity and the homogeneity of the results, due to difficulty of repeating trip experiments when targeting unexpected trips.

2.1. Trip-Inducing Mechanisms

Study about trip-and-fall prevention and intervention devices require the collection and recording of true trip-induced events and thus a tripping mechanism system is needed. The existing studies investigating trip-and-falls used various mechanisms to induce trips. Some studies used a retractable cord attached to the ankle of the participant that can be stopped using a solenoid-driven or other brake system which when activated, clamp the cord between two grooved surfaces to stop trailing foot/leg and therefore induce trip [66].

Other studies equipped each foot with independently controlled device, where the main reason was to maintain symmetry and contribute to the unexpected nature of the gait perturbations, due to subjects not being aware on which foot the trip will be triggered [67-68]. Alternative trip triggering mechanism reported in the existing literature include use of a hidden tripping board in a form of a flapping mechanism that uses springs as storing energy system to spring up suddenly from the walkway and trip the subject when triggered [12].

Similarly, a strategy of using a hinged metal plate positioned flat on the ground and controlled using electromagnets and memory springs was used to trigger trip in [69]. The device was triggered by cutting electricity on the magnets, which made the plate spring upright in to the vertical position by the help of memory springs on both sides of the plate. Furthermore, other studies used treadmill in order to induce trip, participants were instructed to walk with a self-selected pace and the treadmill belt suddenly accelerated in the direction backward when inducing trip is desired [70].

Recently, an apparatus for delivering a trip-causing obstacle directly on a treadmill with precisely-controlled release timing was developed. Other studies used a spring-loaded tripping board that get flipped when an optical foot detector hidden on the side of the walkway is activated in order to induce trip [71].

2.2. Trip Platform Design Requirements and Process

For the purpose of this study to conduct trip experiments, a trip triggering platform was designed to allow testing. The first requirements for the platform design were related to the strength, portability, and compact design. The platform needed to be

long enough that allows subjects to walk multiple steps to achieve normal walking gait have the ability to be portable and stored in a small area after the end of experiments for the purpose of practicality. The second design requirement was the rapid actuation.

The system needed to be faster than the human reflexes in order to trigger trip. In addition, the system need be concealed so that the participant will not be aware of when and where the event will happen in order to obtain their natural walking gait and experience an unexpected trip. The final requirement is that the technology used in the platform triggering mechanism needs to operate efficiently with minimal complexity in order to prevent excessive maintenance or resources and has to be safe, due to working in close proximity to human subjects.

Based on the above requirement, the size of the walkway platform designed for this research was 7 m × 1 m × 0.15 m (length × width × height) to provide the needed space for the participants to walk on a moderately low platform that will allow the implementation of triggering trip system underneath the walkway.

The width of the trip triggering device was only half of the width of the platform, due to the requirement of triggering only swing/trailing leg during the swing portion of the gait. Due to the vertical retraction mechanism of the plate, the trips can be induced on either leg when subject is walking in one or the other direction on the platform. The regular construction wood was chosen as the base material, due to its sufficient strength, low-cost, and ease of fabrication.

For the storage purposes, the walkway of the platform was divided into three panels that can be assembled together using a fixation U-bolts on both sides of each panel plates with different dimension that were already existing in the Biomechanics lab at Rowan University (see Figure 2).

Figure 2

Top View Structure of the Experimental Platform

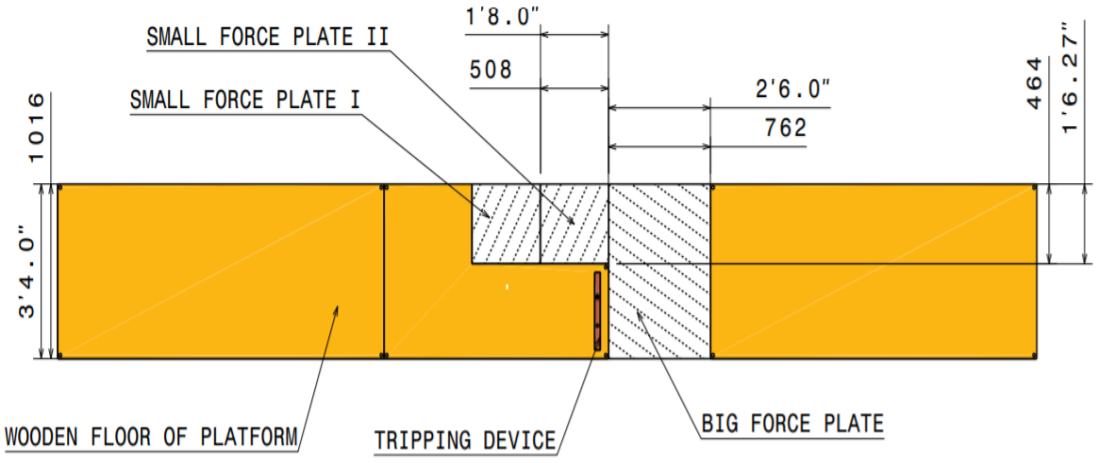

Note. The structure of the platform is constituted by three panels (i.e., I, II, and III) attached by U-bolts from sides. The length of the individual panel was 2.3 m. Three different force plates and their locations are demonstrated in the drawing.

Trip was induced by an obstacle device consisting of a wooden plate of 0.09 m high, 0.5 m wide, and 0.04 m thick. It was equipped with a two-compression loaded spring and guided by two slippery low friction rods from both sides to ensure both

symmetry and guidance of the plate in order to prevent any jamming or disorientation when launched up or when the participant collided with it (see Figure 3).

Figure 3

Cross Section of the Tripping Mechanism and the Latching System

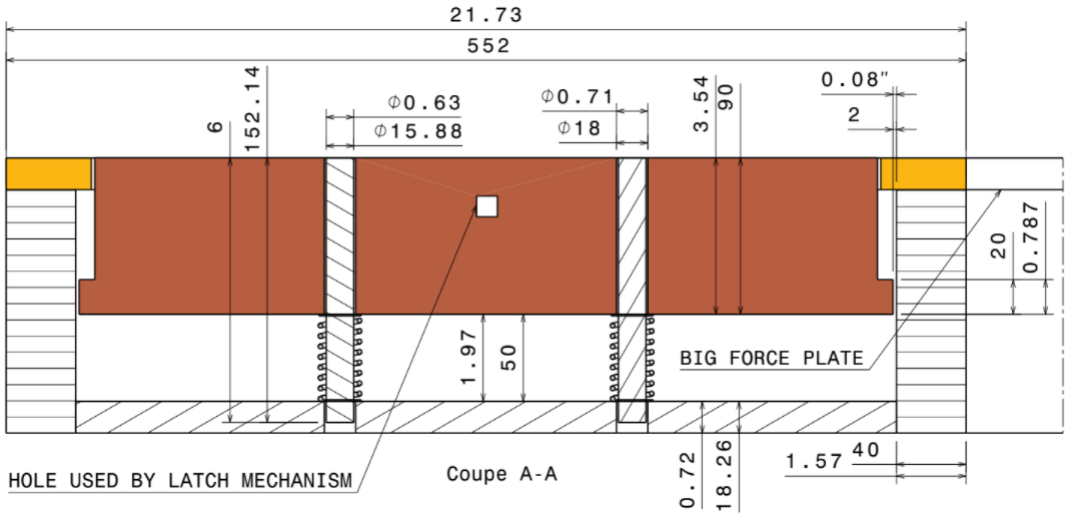

Note. The structure of the tripping mechanism consists of a wood plate driven by two compression loaded springs positioned in the bottom and guided by two slippery low friction rods for symmetry and guidance.

The plate was locked in a vertical position with the help of a latching mechanism consisting of a spring-loaded side bolt latch. During normal walking tests, the top of the plate was hidden and aligned evenly with the rest of the platform in order to make it difficult to localize its location by the subjects, enabling to make the perturbation events as sudden and natural as possible. During a perturbation event, the latch is released using

a rope passing under the platform and controlled by a human observer. At that moment, the plate is raised due to the stored energy in the springs and trip is induced by obstructing the trailing/swing foot of the participant.

The design was first sketched and modeled using a computer-aided design software (CATIA V5 R21). Each panel of the platform was designed separately to allow flexibility of modifications and the precision of the interactions between different components. All the parts were then assembled into one product using the assembly design capability of CATIA V5R21. In addition, a kinematic simulation of the system during the triggering phase was accomplished using the DMU Kinematics library in the CAD software to ensure that all parts of the system are working properly.

Unfortunately, the above-mentioned design was not used as the main platform for trip experiments, due to pandemic and an alternative, simpler solution was sought to perform the experiments. Therefore, the experiments were performed using a rope attached to the heel of the participants to trigger trips by pulling it at specific times. A small load cell was mounted on the foot and attached in series between the foot and the rope to measure the exerted perturbation forces and serve as a validation for the trip onset and duration. Additional reasons and advantages for adopting the latter approach rather than using the platform is that restricting the participant leg using pulling rope techniques is much easier to implement and provides more flexibility for testing setup since no structure needs to be build and fixed in specific place in order to make the experiments.

Using a rope setup is a simpler and more cost-effective solution with additional capabilities to measure the forces exerted on the targeted leg by the intermediate load cell

that was not considered in the first approach. The limitation of using rope to trigger trips is that in this approach the subjects need to drag the rope during the experiments that can potentially influence gait in particularly when the rope is very long. To minimize this effect, we chose a light weight, non-stretchable rope and an observer would carefully feed the rope during the experiments.

2.3. Experimental Protocol, Data Acquisition and Data Post-Processing

2.3.1. *Inertial Sensors Specifications and Configuration*

For the purpose of collecting kinematics data during the experiments, the inertial measurement unit (IMU) system was attached on human body parts. The IMU systems are commonly used in biomechanical studies to measure the human kinematic data, due to their small size, light weight, and being easy to wear.

Figure 4

SparkFun MPU 6050 IMU Sensor

Note. The MPU 6050 sensor electronic board with its different pins and components used in the experimental setup.

The IMU system used in this study consisted of seven 9-degree-of-freedom Sparkfun MPU6050 IMU sensors with 50 Hz sampling frequency mounted on different body segments were used (see Figure 4).

The IMU units are synchronized with each other and data from all of them was collected simultaneously using a Raspberry Pi electronic board featuring quad core 64-bit processor, 4GB RAM with wireless networking connection.

Each Sparkfun IMU electronic board is composed of 3-axis accelerometer capable of providing measurements up to ±12 g, which provides different limb linear accelerations, a 3-axis gyroscope capable of providing measurements up to ±2000 deg/s that provides the angular velocities of the participants' limbs, and a 3-axis magnetometer.

2.3.2. *Load Cell Specifications and Configuration*

The determination of the exact trip onset moment plays an important role in the analysis of the data, since it allows to know at which swing phase portion the trip occurred.

Knowledge about the instance of the gait perturbation onset has an implication for predicting the potential recovery strategy used by the participant as well as allowing to compute of the rapidity of the detection algorithm by taking it as a reference point.

Figure 5

S-Load Cell with Housing Attachments and the Tension Cable

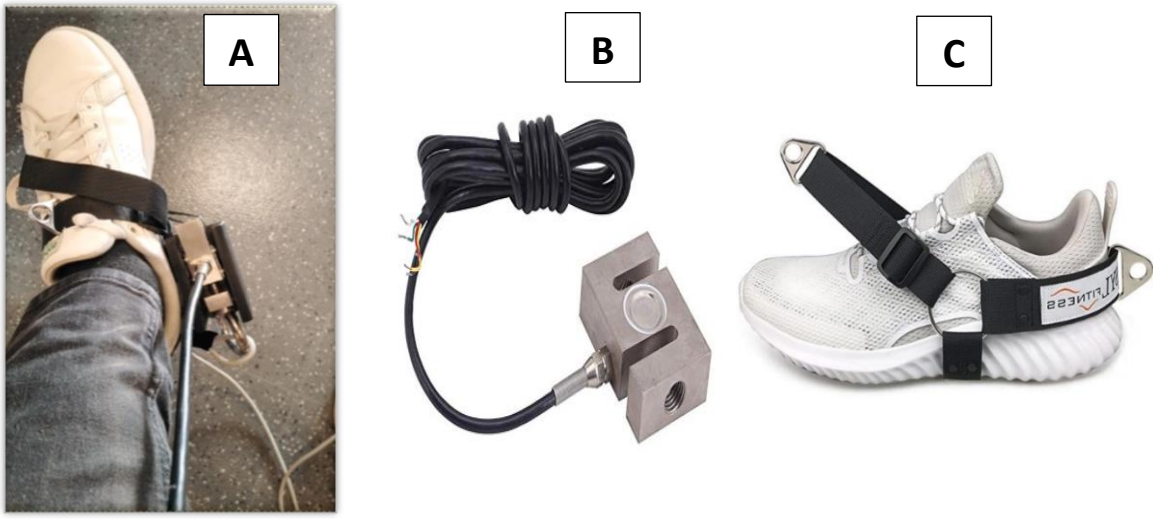

Note. A, The S-load cell inside a custom designed housing attached to the participant's foot using a shoe strap. B, the S-load cell used to determine the trip onset. C, Shoe strap used to mount the housing of the load cell on to the foot.

To establish the detection of the trip onset, a portable S-type beam high-precision load cell (Walfront PSD-S1) with a scale reading up to 981 N was mounted on the participants' ankle using shoe straps and a custom designed housing for that specific purpose (see Figure 5).

A non-elastic rope was attached to one side of the load cell that allowed to apply tension force when pulling the rope to induce trip perturbations. During normal walking, the attached rope was free to move and no significant tension force was applied to the load cell. In the case of trip onset, the rope attached to the load cell was suddenly stopped and the tension force was applied on the load cell for the entire duration of the

obstruction of leg movement, which allows the determination of the trip onset time and duration of trip perturbation.

2.3.3. *Raw Data Post-Processing*

The recorded data from the IMU sensors measuring the subjects' kinematic data during the experimental trials contained the raw output of the accelerometer and gyroscope signals in their local coordinate frames. These measurements were post-processed and analyzed. Compared to the gyroscope sensor, which provides direct measurements of the angular velocities with their corresponding orthogonal axis, the accelerometer readings measure accelerations that include contributions due to dynamic motion and gravity.

Therefore, the readings from gyroscopes are suitable to be applied in diverse dynamic conditions were rotational velocities are introduced, however, its reading tends to drift with time. This drawback affects not only the output signal but also the subsequent computations based on this quantity and thus filtering operations are needed to compensate the low frequency signal drifts.

On the other hand, the accelerometer, which measures linear accelerations in its local coordinate frame, works well in static conditions as opposed to the gyroscope, however, its reading has noise and is affected by vibrations and other external forces. Hence, its output signal cannot be used directly for joint angle computations, therefore, filtering action is required as well in order to remove the dynamic noise accumulated during the trials.

For the filter choice and based on the literature regarding filtering human motion kinematic data, a lowpass 2nd order Butterworth filter with a 6 Hz cutoff frequency was chosen in order to attenuate the noise while preserve the information contained in the sensors output [72-73].

2.4. Subjects Selection Criteria

The human subject testing was performed to collect and analyze the experimental data. Two young male adults volunteered to participate in this study. The selection criteria considered volunteers' health conditions. Requirements including no preexisting record of illness such balance disorder, neuromuscular diseases, or falls neither any history of fall arrest training in order to preserve the natural behavior of human subjects during perturbation onsets. The participants had an average age of 25 ± 3.55 years and average high of 1.76 ± 0.058 m, and an average weight of 79.33± 10.33 kg.

2.5. Experimental Protocol

Both volunteers wore tight sportswear for easy sensor attachment during the testing trials. Before starting the experiments, the subjects were asked to try regain their balance in case of trip occurrence. For security reasons, a safety harness was attached to the shoulders of the participants with addition to wearing the knee pads and ankle joint elastic brace.

Seven IMU sensors with a 50 Hz sampling frequency were fixed on the participants' lower back, left and right thigh, shank and heel. The subjects were instructed

to walk along a 7 m walkway at a self-selected speed. An inelastic rope attached to a S-load cell was used to trigger and determine trip onset.

Trip was induced using a combination of pulling motion and a solenoid-cam cleat rope restriction system to stop the trailing foot at different portions of the swing phase of a gait in order to trigger various recovery responses to trip perturbations, (see Figure 6).

Figure 6

Experimental Setup Used in Trip Experiments

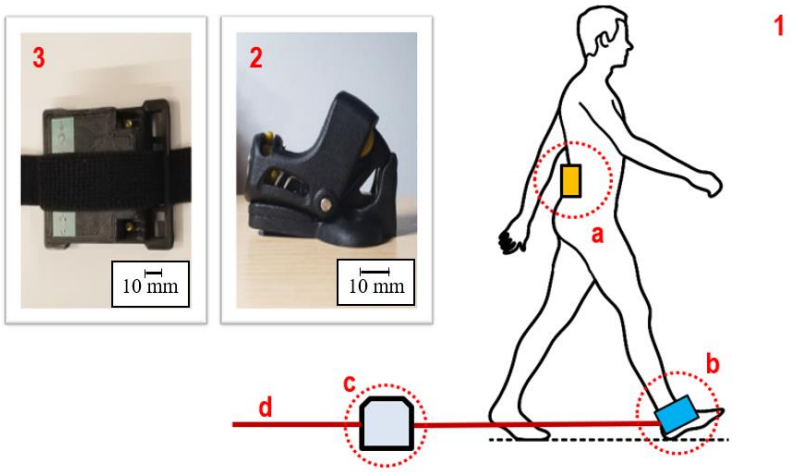

Note. A schematic figure explaining the experimental setup used in the trip trials. 1, General setup configuration. a, IMU sensor. b, S-load cell attachment. c, Cam-Cleat rope restriction device. d, Inelastic rope. 2, Cam-Cleat used as the rope restriction device. 3, Lower back IMU unit used in the experiments to measure trunk angle.

A total of 40 trials were conducted. Among those, 30 of them included trip perturbations induced at different swing phase portions, while the other 10 were normal walking trials that served as a reference in comparison of the kinematic variables. The collected data were verified to ensure the absence of any missing or distorted sensor data and post-processed for later analysis.

2.6. Trip Classifications

Significant amount of research has been carried out about the recovery strategies that individuals employ to avoid fall after a trip and their relationships with the timing of trip onset. [71] Studies concluded that there is a correlation between the trip onset time and the recovery strategy used resulting in three main strategies. The lowering strategy is when the tripped foot is immediately lowered on the ground and acts as a support leg during the recovery phase.

Such strategy was observed only during late swing phase trip perturbation. Elevating strategy is when the tripped foot is immediately raised above the obstacle and the limb accomplishes the recovery. Such strategy was observed only in the early swing phase trip perturbation.

The reaching strategy is very similar to the elevating strategies with a small difference related to the limb flexion, since this strategy it primarily executed at the hip level. Such strategy was observed in mid-late swing phase [74-75].

In this study, trips were classified according to the above-mentioned classification reported in the existing literature. All three main trip categories were considered to perform a comprehensive analysis of trips occurring throughout the whole swing phase.

Early trip is classified if the trip perturbation is induced during the 60% to 70% of the gait (i.e., ~10-40% of swing phase), mid-trip induced during 70% to 85% (i.e., ~40-70% of swing phase), and late trip if trip occurs after 85% of the gait (see Figure 7).

Figure 7

Foot Trajectory During Human Gait with Noted Three Swing Phases

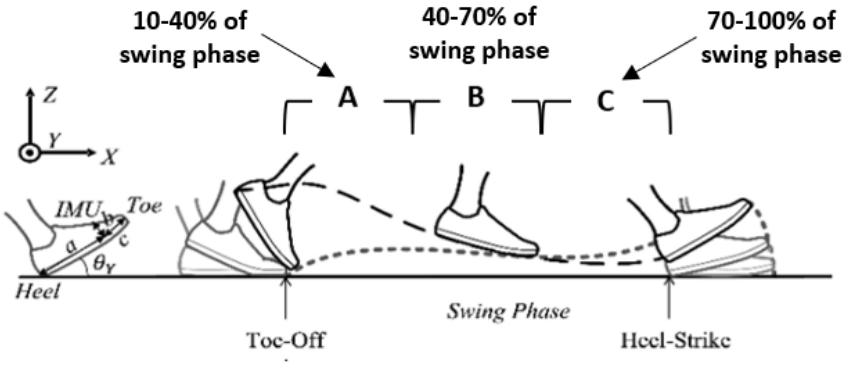

Note. A schematic figure of different gait features and phases of human gait with marked three portions of swing gait corresponding to three trip recovery strategies employed by the subjects experiencing trip. A, Early trip (lowering recovery strategy). B, Mid trip (elevating recovery strategy). C, Late trip (reaching recovery strategy). [76]

2.7. Kinematic Variable Selection

In order to better understand how a trip can be detected, it is imperative to have a comprehensive understanding on the type of data and inclusion of biomechanical parameters, including selection of anatomical joints and their kinematics that need to be considered. The analyses of joint angles as a function of time or gait phase can allow identification of the required joint positions at different gait stages during locomotion to maintain gait stability and normal gait progression.

However, such quantities cannot directly provide any measures of the joints' performance neither the control of movement. Compared to the joint angles, the joint angular velocity measurements provide additional information about how the subject performed joint motions and the corresponding walking gait. However, such data cannot explicitly indicate the smoothness of the movement and it does not yield important information necessary for detection of sudden joint movements.

Joint angular accelerations represent the rate of change of the joint angular velocities and are related to the muscle efforts overcoming inertial forces to either stop or start a movement. Investigating the joint angular acceleration profiles can provide information about the expected trajectory profiles at different gait phases and contain an information about the characteristics of the walking gait.

Deviations from those profiles can indicate a presence of sudden movement abnormalities during walking that can be used for trip detection purposes as considered in this thesis.

During basic walking the hip joints will experience an abduction and adduction movement in addition to flexion and extension, while the knee and the ankle joints will primarily experience a flexion and extension movements.

When abnormal obstruction of walking movement occurs at the foot level as in the case of a trip, the perturbation transferred proximal to the center of mass and a sudden angular acceleration at the hip joint level is observed that is caused by the sudden shifting of the body's center of mass and a forward rotation of the trunk. Therefore, monitoring and analyzing the angular acceleration profiles of the lower back can provide information about trip perturbations and falls

Chapter 3

Threshold-Based Trip Detection Methods

In this chapter, three threshold-based trip detection methods are described that were developed to detect trip during walking in the shortest possible time after the trip onset. The approach relies on using a wearable IMU system to allow trip detection in the everyday environment. Trip events introduce perturbations in the human body kinematics compared to normal walking, which lead to deviations in many human kinematic variables, including the motion of the trunk.

Therefore, the proposed trip detection methods described in this thesis rely on detecting changes in human trunk kinematics and quantify them in a fast and efficient manner. The first method is based on the angular jerk (J) of the lower back in the sagittal plane serving as the main trip indicator. The angular jerk (J) is obtained by direct double integration of the angular velocity measurements from a single IMU mounted at the lower back. The second method is based on the computed quadratic mean (i.e., root mean square (RMS)) of the angular acceleration signal of the lower back ($\ddot{\theta}$). The third method uses a statistical measure of the magnitude of the lower back angular acceleration also known as signal magnitude area (SMA).

The trip detection algorithm was designed based on the fixed threshold of all three individual parameters taken as the maximum value of the two-standard deviation (2σ) envelope obtained from normal walking trials across both subjects. Trip was detected when the real time measured signal surpassed the threshold value related to the jerk method, RMS method, and SMA method, respectively. For all three methods, the desired

trip detection time was under 100 ms, which is faster than the human voluntary reactions (~200 ms) [77]. The algorithms capabilities of such rapid trip detection would be useful for the real-time implementation of active trip-and-fall prevention devices and systems.

3.1. Angular Jerk Method

In order to detect trip, it is essential to select a kinematic parameter that can be used to detect the abnormal changes in the body movements caused by tripping. The lower back angular jerk can potentially provide the needed sensitivity to detect such abnormalities, due to previous studies showing that the changes of the back angle in the sagittal plane are correlated with the trip onset.

Angular jerk (J) is defined as the rate at which the angular acceleration ($\dot{\theta}$) changes with respect to time. Measuring angular jerk of anatomical joint can provide a vital information about how smooth the human movement is, as it is very sensitive to the sudden changes in the resultant forces affecting the motion and the resulting changes in the accelerations [78]. Analyzing angular jerk (J) signals of the lower back can be utilized to detect sudden abnormalities in subjects' trunk movement when compared to a normal walking signal. From a mathematical perspective, the angular jerk (J) is defined as

$$J = \frac{d^3\theta}{\mathrm{dt}^3} \tag{1}$$

where θ represents the angular displacement of the lower back. Figure 8 shows the trip detection decision tree algorithm using the angular jerk as the main indicator. The algorithm flow is as follows.

The first step consists of initializing the size of the sliding window that defines the vector length of the analyzed signal used in post-processing or in real-time applications. The second step consist of filtering the raw data coming from different IMU sensors and load cell to remove noise from the signal that can affect the calculation and the system detection algorithm.

A threshold value (J_{tr}) is introduced in the next step of the algorithm to make a decision about the instance of trip occurrence by comparing and identifying when the measured signal exceed the threshold.

The threshold value (J_{tr}) was taken as the maximum value of the two-standard deviation (2σ) envelope obtained from several normal walking trials as shown in Figure 9. Trip was detected when the measured signal surpassed the threshold values of J_{tr}= 1600 m/s^3.

To test the efficiency of the proposed algorithm, a total of 30 trip trials from two participants with trips triggered at different swing phases (i.e., early 60-70%, mid 70-85%, or late trip 85-100% of gait), were collected and analyzed to evaluate how fast and accurately the algorithm detects trip events across all collected trip trials.

Figure 10 present trip trial for the early, mid, and late trip occurrences with respect to normal walking behavior. Marked are key instances, including the heel strike, the toe-off, trip onset instance, trip detection time, and the two-standard deviation (2σ) threshold discussed above.

The results show that during normal walking the angular jerk values observed are below the two-standard deviation threshold.

Figure 8

Trip Detection Decision Tree Algorithm Based on Lower Back Angular Jerk Measurements

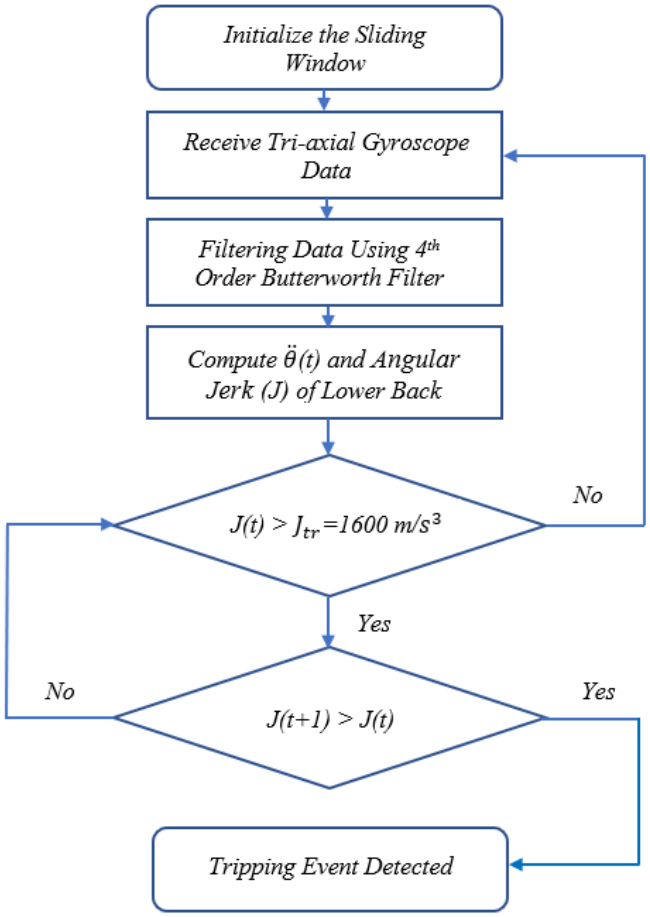

Note. The algorithm indicates trip was detected if the angular jerk signal exceeds the two-standard deviation threshold and continues to increase.

During the stance portion of the second step before the perturbation was induced, the rate of change of the angular jerk follows the expected trend, similar to that during normal walking, which indicates that the trunk movement is controlled and no sudden perturbation or force is being applied on the human body.

Soon after the toe-off instance, when the trip perturbation is induced, the angular jerk sharply increases and exceeds the threshold, hence the trip is detected.

Figure 9

Mean and Two-Standard Deviation (2σ) Envelope of the Lower Back Angular Jerk Signal During Normal Walking

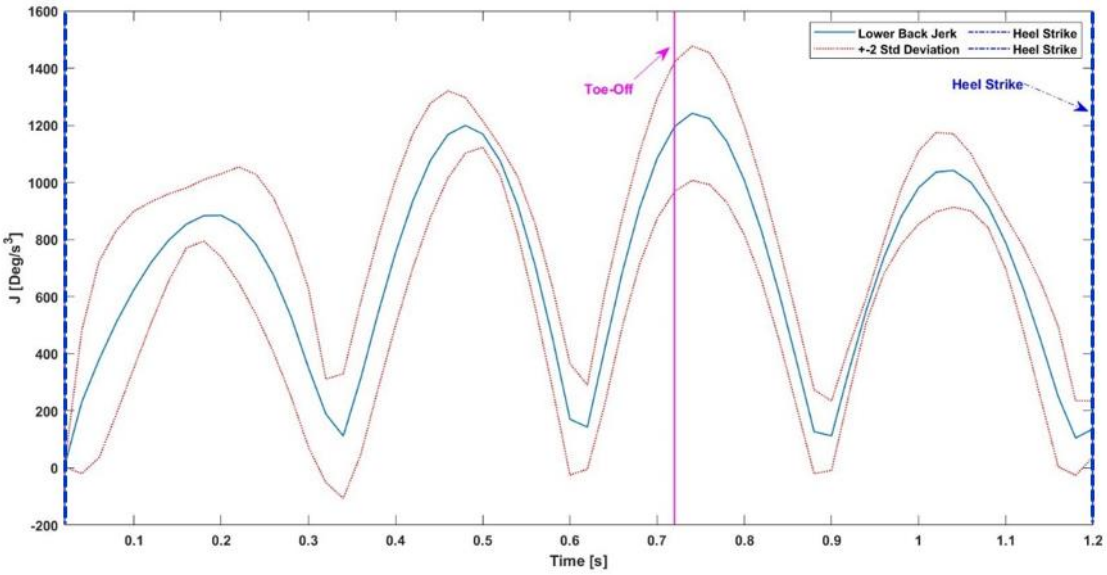

Note. The mean (blue) lower back angular jerk signal of ten trials during normal walking with a two standard deviation envelope (red) and marked toe-off instance (magenta).

Figure 10

Lower Back Angular Jerk During Normal Walking and Early, Mid and Late Trip

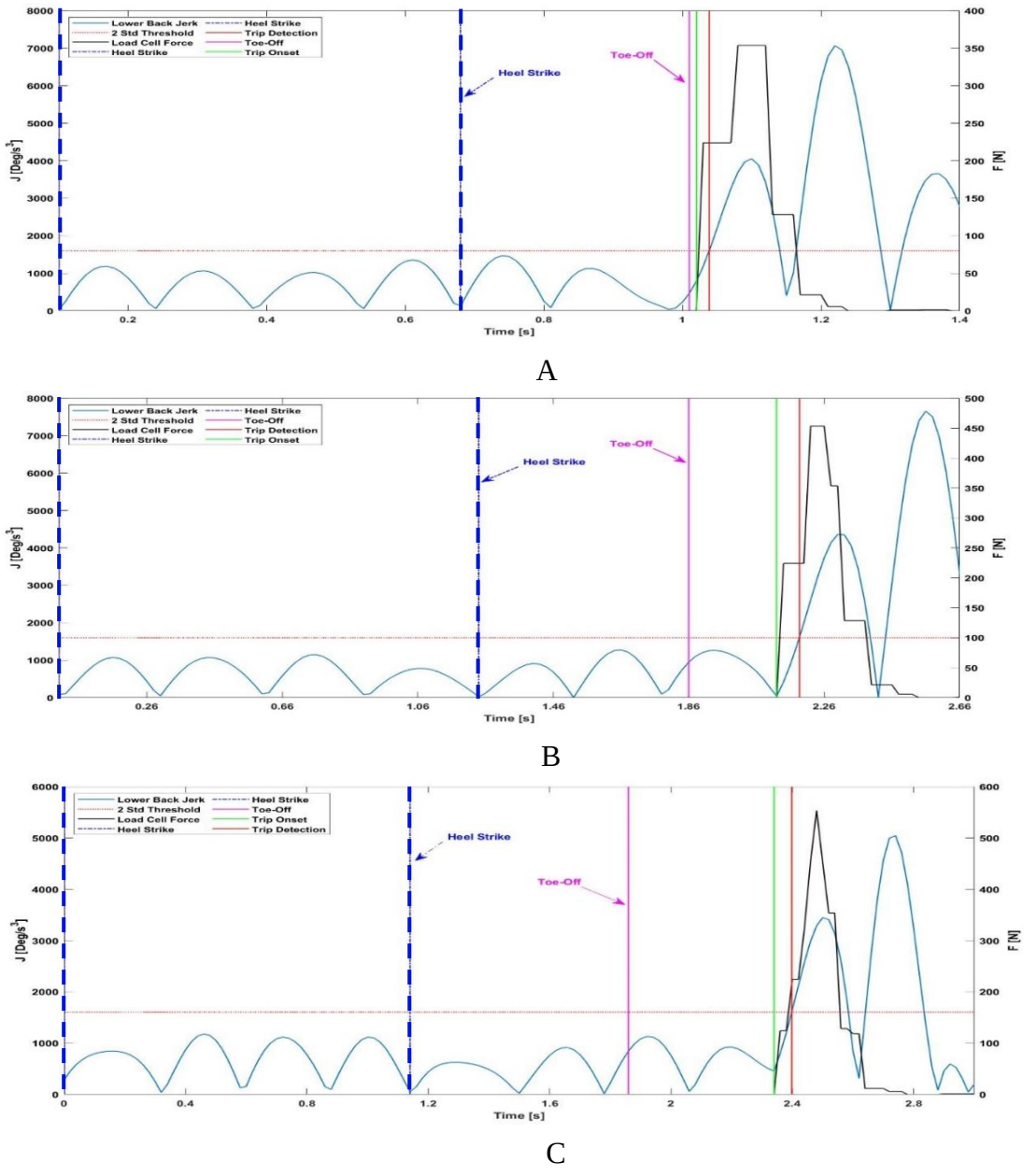

Note. Presented are two full steps, first one being normal walking and second includes trip event for the case of A, an early trip, B, mid-trip, and C, late trips with trip detection times of 30 ms, 55 ms, and 50 ms, respectively.

During the stance portion of the second step before the perturbation was induced, the rate of change of the angular jerk follows the expected trend, similar to that during normal walking, which indicates that the trunk movement is controlled and no sudden perturbation or force is being applied on the human body. Soon after the toe-off instance, when the trip perturbation is induced, the angular jerk sharply increases and exceeds the threshold, hence the trip is detected.

Figure 11

Comparison of the Trip Detection Times (Mean and Standard Deviation) Across Both Subjects for the Angular Jerk-Based Algorithm

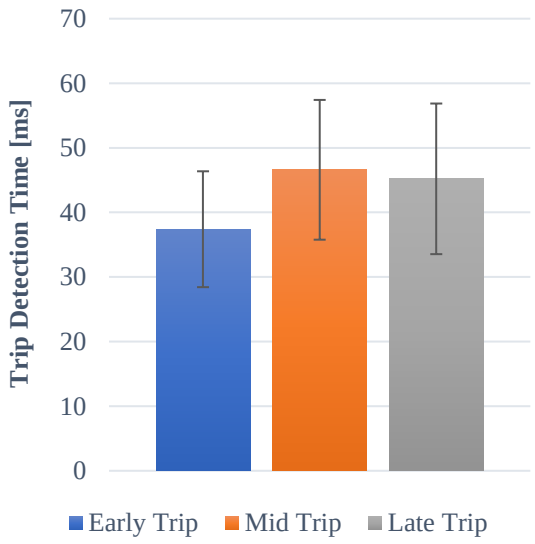

Note. Results of the average detection times across both subjects for the early, mid, and late trips with the largest mean trip detection time of 46.6 ms during mid trip and the shortest detection time of 37.4 ms during an early trip.

Figure 11 shows results of the average detection times across both subjects for the early, mid, and late trips. The results show that the proposed algorithm can detect trip events efficiently with the overall mean time of 43 ms and a detection rate of 100% across all trials including different trip onset timings. The detection time is much shorter compared to the human voluntary reaction time to trip perturbations [78]. Therefore, the developed system can be possibly integrated in an assistive device for trip balance recovery, where it is necessary to detect trip immediately after trip onset allowing any actuated mechanical systems to provide assistance in adequate timing to prevent a fall.

3.2. Signal Magnitude Area Method

The second proposed trip detection method relies on using a signal magnitude area (SMA) of the trunk angular acceleration as the main trip indicator. This method has been previously used to detect daily physical activities from accelerometer signals based on human posture in healthy and amputated individuals, although has never been used in order to detect trip perturbation as proposed in this thesis [79-80]. SMA is a statistical method that measures the magnitude of variation of a continuous-time waveform quantity using normalized integration of the original values. SMA is mathematically defined as

$$SMA = \frac{1}{N} \left| \int_0^N \ddot{\theta}(t)\, dt \right| \tag{2}$$

where N is the length of frames (N=5) in the sliding window that is equivalent to (N =100 ms) considering our sampling frequency of 50 Hz (dt=20 ms). For the purpose of trip detection using the SMA as a main indicator, the detection algorithm flow is as follow.

The first step consists of initializing the sliding window by providing the width of the window and specifying its type (i.e., overlap or translating). The selection depends on the frequency components of the measured signal in order to provide a good resolution of the SMA as input into the algorithm.

Figure 12

Mean and Two-Standard Deviation (2σ) Envelope of the Lower Back Signal Magnitude Area During Normal Walking

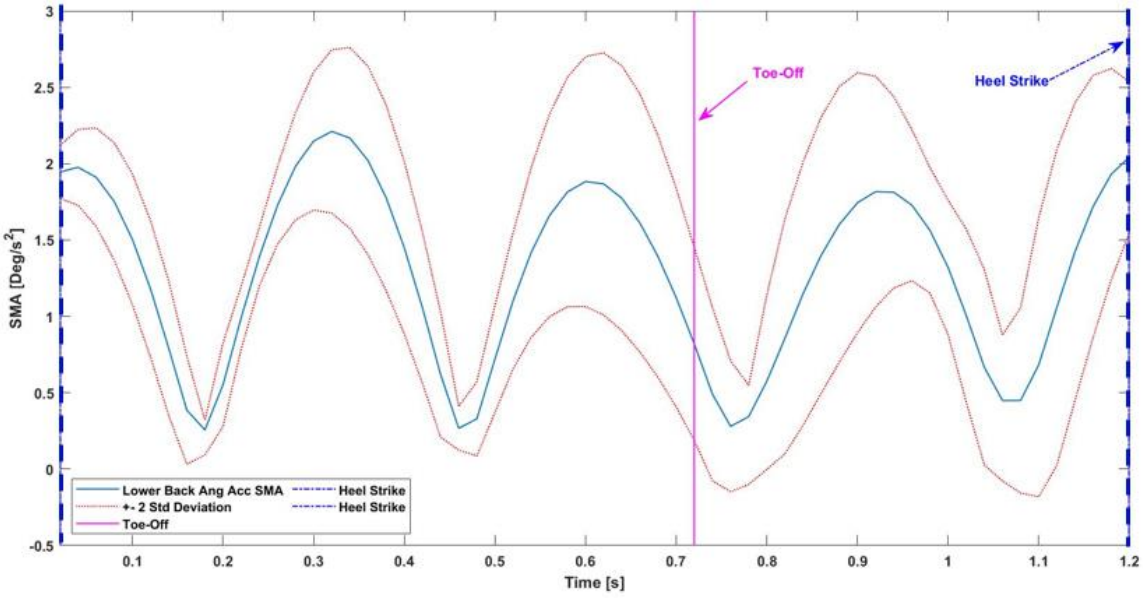

Note. The mean (blue) lower back signal area magnitude of 30 trials during normal walking with a two standard deviation envelope (red) and marked toe-off instance (magenta).

Figure 13

Trip Detection Decision Tree Algorithm Based on Signal Magnitude Area

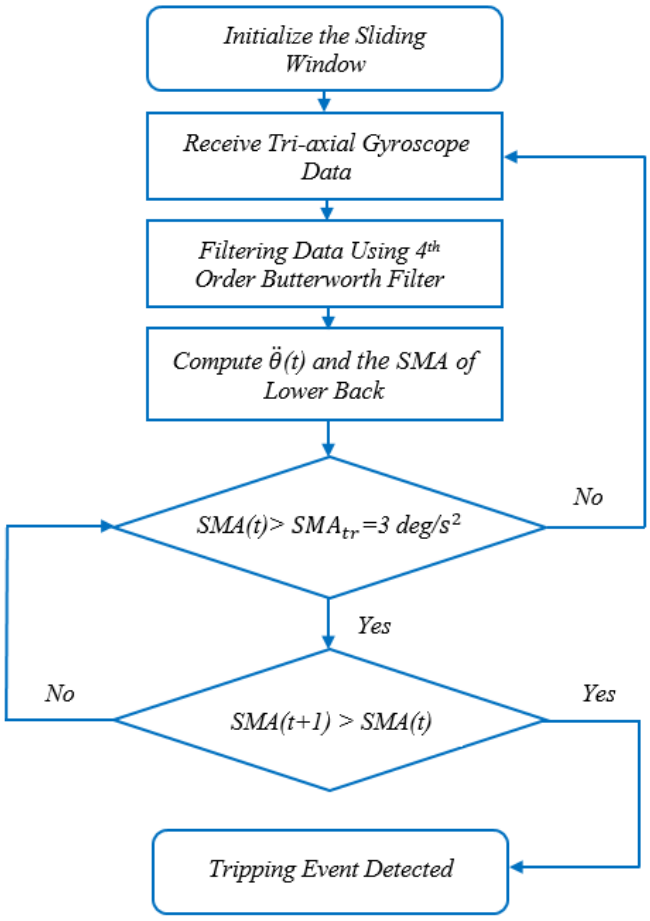

Note. The algorithm determines the trip onset and duration when the SMA of the lower back angular acceleration signal exceeds the two-standard deviation threshold (SMA_{tr}) and continues to increase.

Figure 14

Lower Back Signal Magnitude Area During Normal Walking and Tripping for the Case of Early and Mid Trip

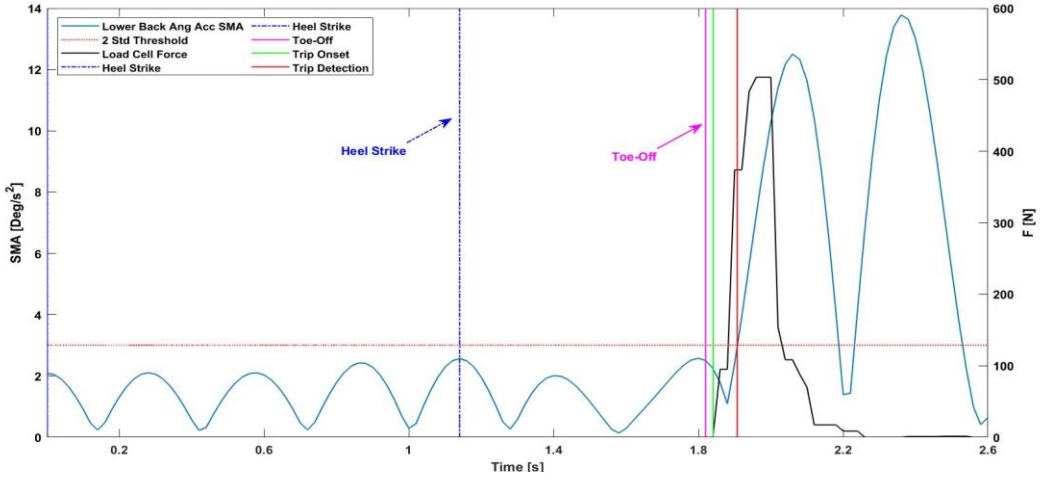

A

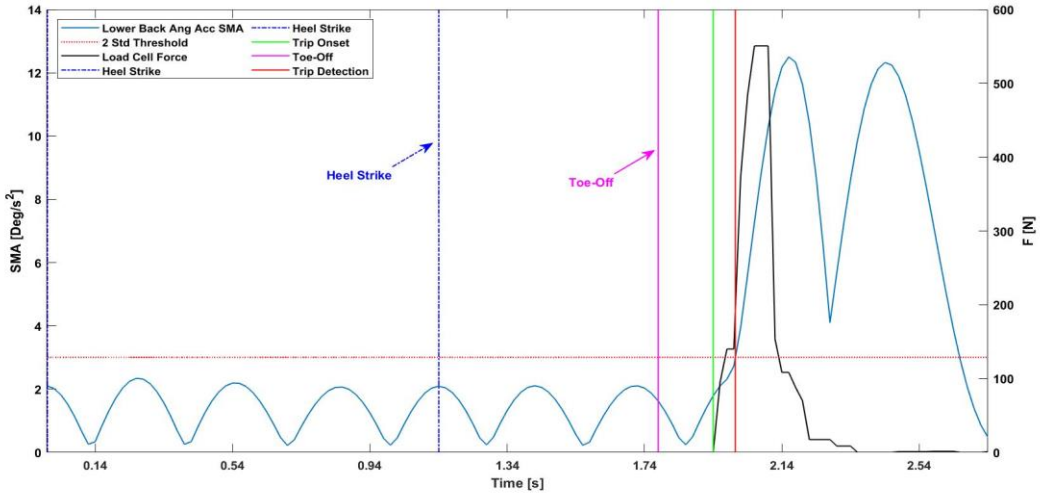

B

Note. Results for two complete consecutive steps are shown in both plots with the first one being normal walking and the second one including trip perturbation. Normal walking and tripping for the case of A, early trip with trip detection time of 65 ms and B, mid-trip with trip detection time of 60 ms.

SMA is computed for the previous N frames of the measured trunk angular acceleration signal during prost-processing or last N frames in real-time implementation. In the next step, raw data from the IMU sensors are filtered to remove noise that can affect the reliability of the system detection. A 4th-order Butterworth filer with a 3 Hz cutoff frequency was used to filter the data. A threshold value (SMA_{tr}) is introduced in the algorithm in order to determine the trip onset.

Figure 15

Lower Back Signal Magnitude Area During Normal Walking and Tripping for the Case of Late Trip

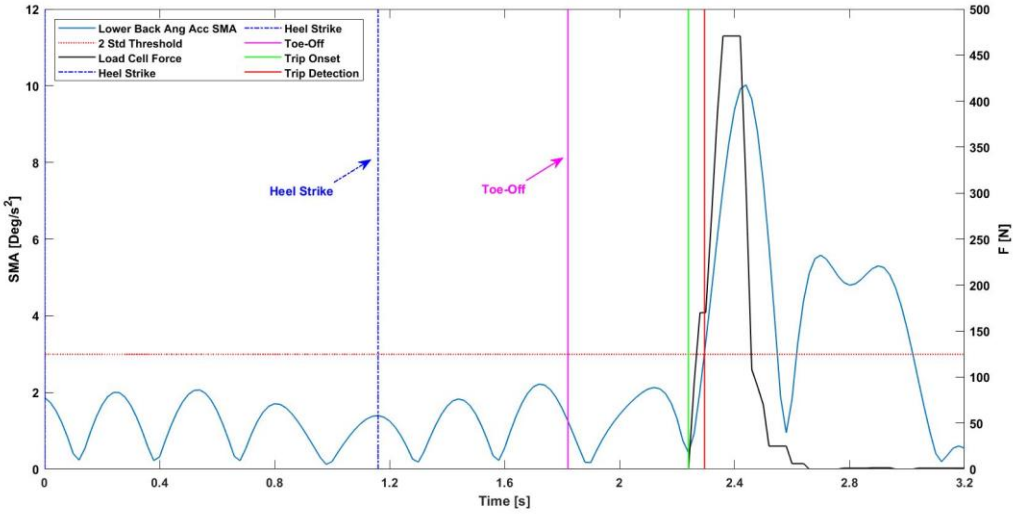

Note. Results for two complete steps are presented with the first one being normal walking indicated between the two dashed blue lines, while the second portion of plot include a trip event. For this late trip trial, trip was detected in 48 ms.

Trip onset was detected when the SMA of the measured signal exceeds the threshold values (SMA_{tr}).

The threshold value SMA_{tr}=3 deg/s^2 was taken as the maximum value of the two-standard deviation (2σ) envelope obtained from ten normal walking trials of the subjects as shown in Figure 12.

Figure 16

Comparison of the Trip Detection Times (Mean and Standard Deviation) Across Both Subjects for the Signal Magnitude Area Algorithm

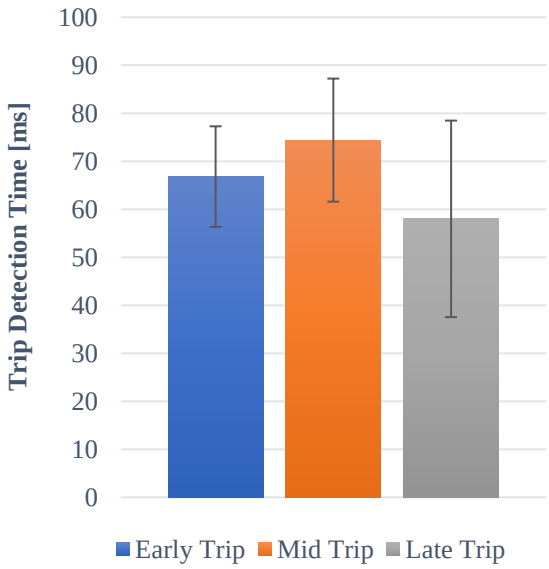

Note. Mean trip detection time across both subjects for the early, mid and late trip had the largest observed mean value of 74.4 ms for mid trip and the shortest for late trip with58 ms.

Figure 13 visualizes the decision tree of the developed detection algorithm using the SMA as a main indicator. Figures 14 and 15 show trip detection results using the SMA-based algorithm for three typical trip perturbation trials (i.e., early, mid, and late trips). Included are key gait features

The actual trip onset and detection instance, as well as the force reading from the S-load cell that serves as a validation of true exerted trip perturbation. The results of the SMA-based trip detection algorithm show that during normal walking behavior the mean SMA of the angular acceleration is under the threshold limit with a periodic trend, which both indicate the absence any abnormal joint kinematics due to perturbation. As soon as the perturbation occurs, the SMA values increase dramatically and exceed the threshold value, hence trip is detected.

Figure 16 shows the summary of trip detection times using the SMA-based algorithm for all recoded trip trials. The mean value of trip detection across early, mid, and late trips with various perturbation lengths was 66.4 ms with 100% detection rate, which shows the effectiveness and efficiency of the algorithm. The average detection time is approximately one quarter of the human voluntary reaction time to gait perturbations [78]. Therefore, the algorithm has the potential to be implement in future human balance recovery systems that help prevent falls.

3.3. Quadratic Mean Method

The quadratic means of a function, also known as a root mean square (RMS), is a mathematical tool that is used to compute the average power of the measured angular acceleration signal. RMS has been used in wide range of application including gait

analysis and biomedical research [82]. The quadratic means of the lower back angular acceleration $\ddot{\theta}$ defined in the sliding window interval $T1 \leq t \leq T2$ can be expressed as

$$\ddot{\theta}_{\mathrm{RMS}} = \sqrt{\frac{1}{(T2 - T1)} \int_{T1}^{T2} \left|\ddot{\theta}^2\right| dt} \tag{3}$$

The simple computation process of the RMS represents an attractive approach to obtain the characteristics of the signal pattern, due to the fact that it does not require any signal preconditioning or analysis (e.g., an accurate signal peak detection).

The physical meaning of the quadratic mean values presents the average of the magnitude of the lower back angular acceleration as a function of a sliding window and thus can be used effectively for the purpose of trip perturbation detection.

It is interesting to notice that for periodic functions like the case of the lower back angular acceleration, the RMS value over all the time of the trial during normal walking is equal to the RMS of one gait cycle [83].

The trip detection algorithm using RMS is similar to those described in previous sections by starting with determining the width and type of a sliding window and then reading and filtering the raw IMU data. A fixed threshold is introduced to provide a reference for trip detection.

Figure 17

Mean and Two-Standard Deviation (2σ) Envelope of the Lower Back Angular Acceleration Quadratic Mean During Normal Walking

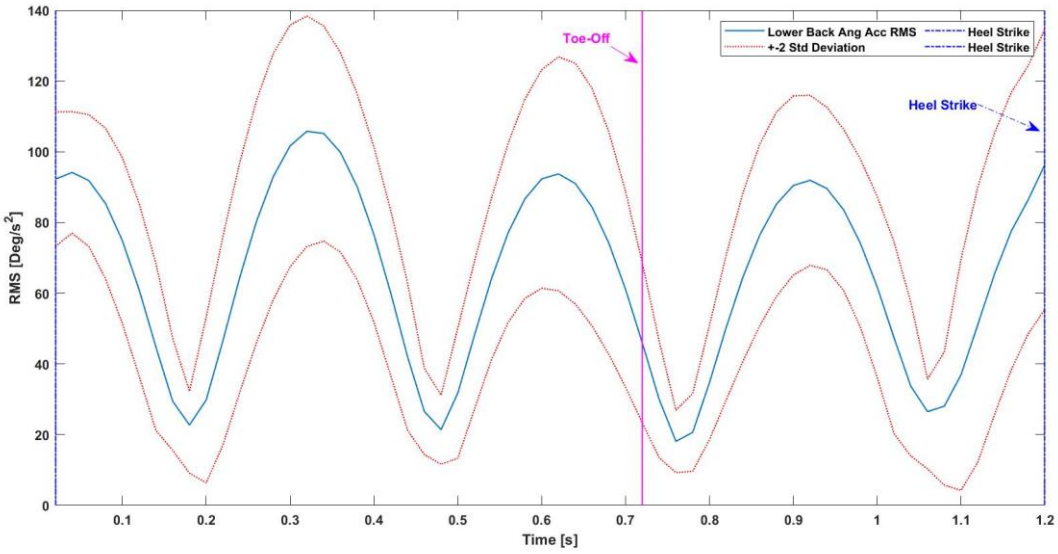

Note. The mean (blue) lower back angular acceleration signal using quadratic mean of ten trials during normal walking with a two standard deviation envelope (red) and marked toe-off instance (magenta).

Trip was detected when the real time measured signal surpassed the threshold value of RMS_{tr}=1500 deg/s^2. Figure 18 shows the visualization of the decision tree of the developed detection algorithm using RMS as a main indicator.

Figures 19 and 20 show results of the lower back angular acceleration quadratic mean (RMS) during normal walking and trip gaits.

Three representative profiles of RMS and the performance of trip detection algorithm for the early, mid, and late trip are presented.

Figure 18

Trip Detection Decision Tree Algorithm Based on The Quadratic Mean

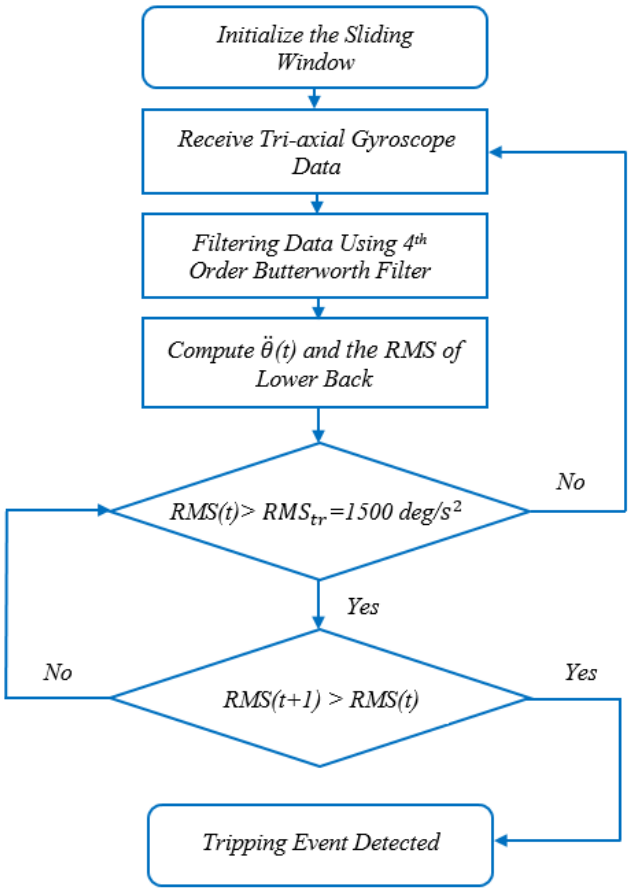

Note. The trip event is detected if the quadratic mean of the lower back angular acceleration signal exceeds the (2σ) threshold and keep increasing in the next instance.

Figure 19

Lower Back Angular Acceleration Quadratic Mean During Normal Walking and Tripping for the Case of Early and Mid- Trip

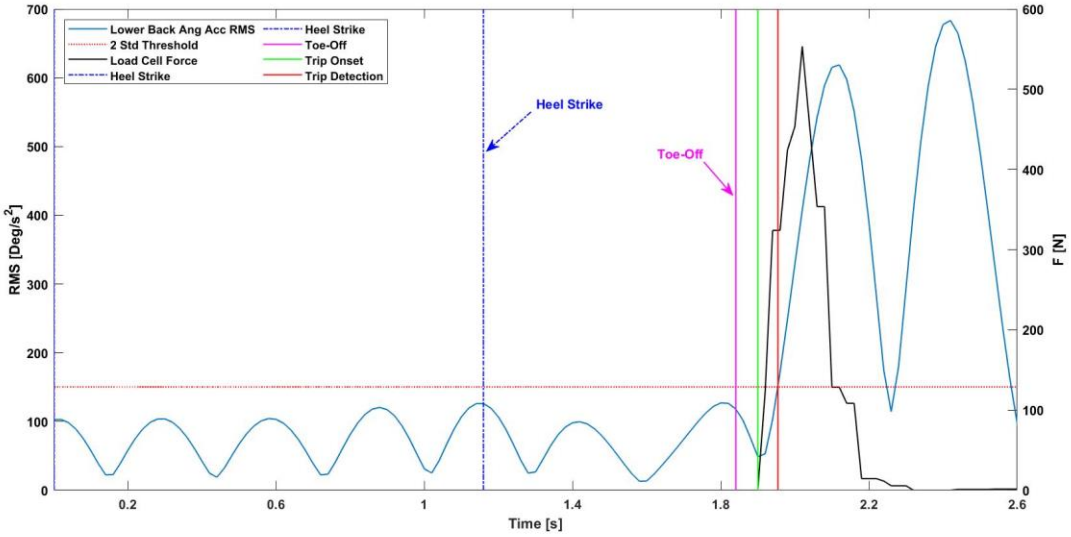

A

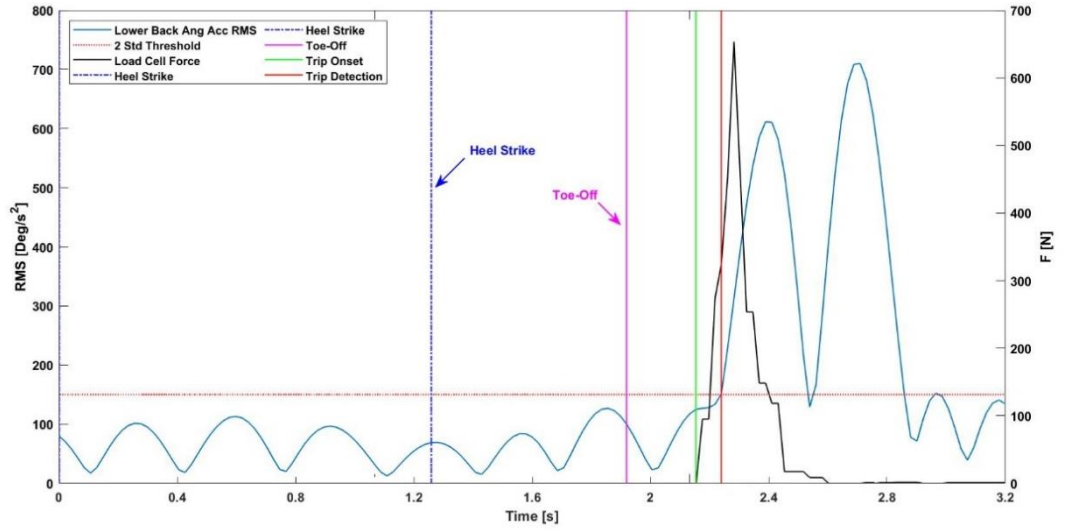

B

Note. Results of $\ddot{\theta}(t)$ RMS values for two total steps in both plots with the first one being normal walking and the second one including trip disturbance. Normal walking and tripping for the case of A, early trip with trip detection time 58 ms and B, mid-trip with trip detection time of 70 ms.

Figure 20

Lower Back Angular Acceleration Quadratic Mean Signal During Normal Walking and Tripping for the Case of Late Trip

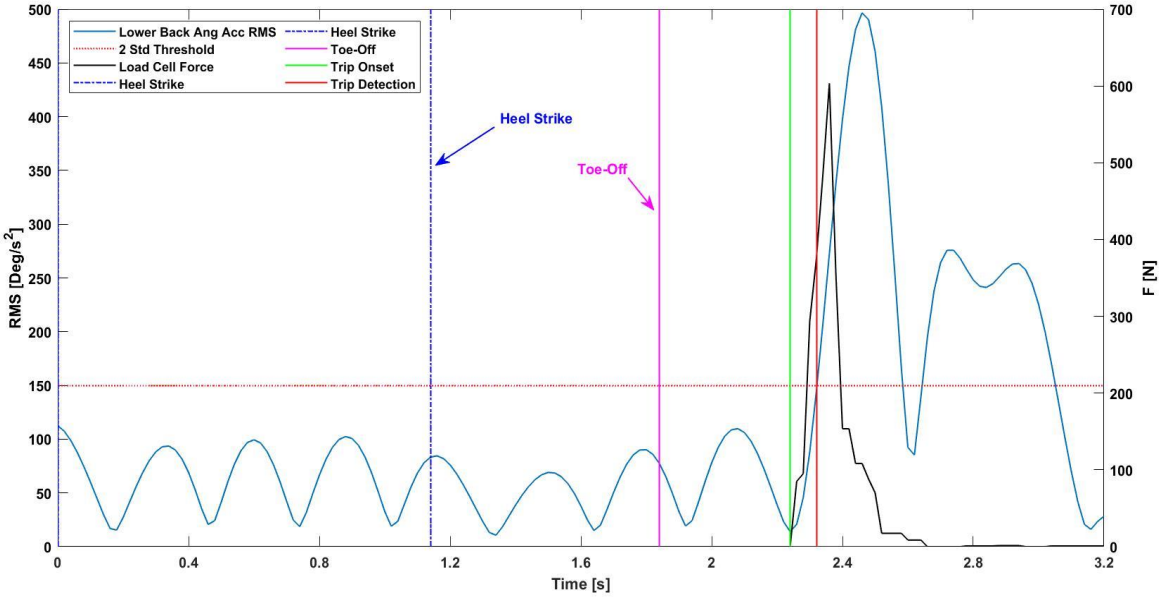

Note. Results for two complete steps are presented in the plot with one the first one being normal walking indicated between the two dashed blue lines, while the second portion other of plot include a trip event. For this specific late trip trial, trip was detected in 68ms.

The threshold was determined as the maximum value of the two-standard deviation (2σ) envelope obtained from normal walking trials of both subjects as shown in Figure 17. The results of the computed RMS values during the normal walking (i.e., portion before labeled toe-off event) exhibit a repetitive pattern which indicates that the movement is harmonic.

The values of the RMS oscillatory profile are below the two-standard deviation(2σ) threshold value. An increase in the RMS values is observed immediately after the trip onset surpassing the threshold value.

The computed RMS values further increase until force form the load cell is reduced to almost zero. Hence trip is detected and the duration of the trip can be estimated until the RMS reaches its first peak value indicating termination of trunk flexion.

Figure 21

Comparison of the Trip Detection Times (Mean and Standard Deviation) Across Both Subjects for the Quadratic Mean Algorithm

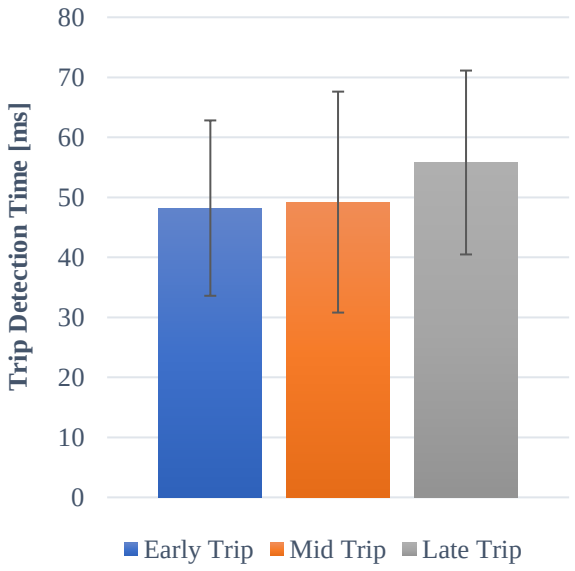

Note. Between both subjects and for the early, mid and late trip the biggest observed mean value was 55.8 ms while the smallest was 48.2 ms.

Figure 21 shows the summary of trip detection times quadratic mean algorithm for early, mid, and late trips. The mean value of trip detection times across all recorded trip data with various perturbation lengths was 51.0 ms with 100% detection rate, which shows the effectiveness and efficiency of the algorithm.

3.4. Elastic Time-Series Alignment Trip Detection Method

All three methods mentioned in the previous sections showed high effectiveness in detecting trip during normal walking. Their advantages are simple integration and fast computational speed making them attractive methods to use. However, their limitation are exposed when dealing with a constantly changing environment where the IMUs cannot provide contextual information. For example, a sudden change in the walking speed (i.e., from normal to slower or faster pace) or bending to pick up an object.

Such changes will provide a wide variation in the signals coming from the IMU sensors compared to the normal walking and the fixed threshold-based methods cannot be used to distinguish between the entire spectrum of human motions and trip-and-falls. Thus, there is a need to use an alternative approach that can provide same effectiveness as previous methods, while overcome their limitation, which can be potentially accomplished using the elastic time series alignment domain.

3.4.1. *Dynamic Time Warping*

Dynamic time warping (DTW) is a time series analysis tool commonly used in voice recognition and machine learning domain. [84] DTW allows to measure the similarities between two sequences of signal and provides an optimal alignment between

both of them even if the signals vary in speed and/or length. Dynamic time warping concept is based on the minimization of the effects of shifting and/or distortion in time through the optimization of a cost function. DTW provides an elastic transformation of time series that allows signal comparison and allows detection of similar signal shapes with different phases. To demonstrate the principle of DTW for trip detection for a chosen measurable variable (i.e., lower back angular acceleration), we consider a lower back normal walking signal $\ddot{\theta}_N := (x_1, x_2, \dots, x_N)$ of length N ∈ ℕ and a tripping signal $\ddot{\theta}_T := (y_1, y_2, \dots, y_M)$ of length M ∈ ℕ. If both signals take values from the same feature space ϕ than in order to compare both signals $\ddot{\theta}_N, \ddot{\theta}_T \in \phi$, it is necessary to compute a local Euclidian distance measurement d_E between individual elements of both signals, which can be defines as

$$d_E: \phi x \phi \qquad \mathbb{R} \geq 0. \tag{4}$$

The distance d_E has small values if both signals are similar and large values if they are different. The local distance in dynamic programming is called cost function [85] and in order to best align the normal walking and trip signal all the points included in both signals need to be arranged in order to minimize the cost function.

Let $C \in \mathbb{R}^{NXM}$ represent the local cost function for all pairwise distances between the individual elements of the $\ddot{\theta}_N$ and $\ddot{\theta}_T$ vector signals, then the local cost matrix for the alignment purpose of both the normal walking and the trip signal can be mathematically presented as

$$c(i,j) = \sqrt{(x_i - y_j)^2}\,, i \in [1:N], j \in [1:M], \quad (5)$$

where $c(i,j)$ represents an individual element in a C matrix. Once the local cost matrix between all different point of the two signals is built, the alignment path between $\ddot{\theta}_N$ and $\ddot{\theta}_T$ can be calculated and considered as a sequence of points $p := (p_1, p_2 \ldots p_k)$ with $p_l = (p_i, p_j) \in [1: N] \times [1:M]$ for $l \in [1: K]$ which must satisfy a few conditions.

The first one is the boundary conditions with $p_1 = (1,1)$ and $p_k = (N, M)$, which implicates that the start and the end points of the two signals need to be aligned together.

The second condition is the monotonicity condition, where $n_1 \leq n_2 \leq \cdots \leq n_k$ and $m_1 \leq m_2 \leq \cdots \leq m_k$, which implies the ordering of the points from both signals must be preserved with respect to time placement. The last condition that needs to be satisfied is called step size condition were $(p_{l+1} - p_l) \in \{(1,1), (1,0), (0,1)\}$ which limits the warping path from large shifts in time during the optimization process. The cost function associated with the optimal warping path computed with respect to the local cost matrix can be expressed as

$$c_p(\ddot{\theta}_N, \ddot{\theta}_T) = \sum_{k=1}^{j} c\,(x_{nl}, y_{ml}) \quad (6)$$

where $c\,(x_{nl}, y_{ml})$ presents the local cost element of the optimal path correlating the element x_{nl} of $\ddot{\theta}_N$ and y_{ml} of $\ddot{\theta}_T$ and the dynamic time warping distance function can then be computed as

$$DTW\ (\ddot{\theta}_N, \ddot{\theta}_T)\ = c_{p^*}(\ddot{\theta}_N, \ddot{\theta}_T)\ =\ \min\{\ c_p(\ddot{\theta}_N, \ddot{\theta}_T), p\ \in\ P^{NXM}\ \},\qquad (7)$$

where P^{NXM} presents the set of all possible warping paths and p^* presents an optimal warping path between $\ddot{\theta}_N$ and $\ddot{\theta}_T$ that have minimal total cost among all possible warping paths. The built accumulated cost matrix D is defined as

$$\text{First Row: } D\ (1, j) = \sum_{k=1}^{j} c\ (x_1, y_k), j\ \in\ [1{:}\ M] \qquad (8)$$

$$\text{First column: } D(i, 1)\ =\ \sum_{k=1}^{i} c\ (x_k, y_1), i\ \in\ [1{:}\ N] \qquad (9)$$

All other elements: $D\ (i, j) = c(x_i, y_j) + \min\{D\ (i\text{-}1, j\text{-}1), D\ (i\text{-}1, j), D\ (i, j\text{-}1)\}$ (10)

Using the DTW, it is possible to gauge the similarity between the normal walking signal and the trip signal in order to identify when the changes due to the trip occur even when the signals do not share same alignment in terms of frame length. For example, if we consider same sampling frequency of data but different walking speed of a subject, then the length of data collected during respective gait cycles will be different. In the following subsection we provide an alternative method to overcome this limitation.

3.4.2. *Dynamic Time Warping Optimization for Trip Detection*

The standard version of the dynamic time warping provides a good solution for analyzing our trip detection problem when post-processing the data. However, the method cannot be directly applied for real-time implementation due to the boundary conditions of both signal in the algorithm (i.e., both beginning and end points of both signals) need to match, which is rarely the case in real-time applications. During real-time

data streaming, the signal of interest starting from the heel strike event is updated as a function of time with new points being added continuously. Therefore, an optimization is needed for the algorithm to make it adaptable for our trip detection purposes and provide the capability to align and match any portion of a tripping signal when compared to the full normal walking gait cycle.

Similarly, as defined in Section 3.4.1., a full normal walking gait cycle signal is defined as $\ddot{\theta}_N := (x_1, x_2, \dots, x_N)$ of length $N \in \mathbb{N}$ and a part of a tripping signal is $\ddot{\theta}_T := (y_1, y_2, \dots, y_M)$ of length $M \in \mathbb{N}$. Different than before, the length of signals is $N \gg M$. Let's fix a local cost function c with the goal to find a subsequence $\ddot{\theta}_T\,(a^*: b^*) := (y_{a^*}, y_{a^*+1}, \dots, y_{b^*})$ with $1 \leq a^* \leq b^* \leq M$ that minimizes the DTW Euclidian distance to $\ddot{\theta}_N$ over all subsequence $\ddot{\theta}_T\,(a^*, b^*)$. Mathematically we express it

$$(a^*, b^*) = \underset{(a,b):\, 1 \leq a \leq b \leq M}{argmin} \{DTW(\ddot{\theta}_N, \ddot{\theta}_T[a:b])\} \tag{11}$$

The indices a^* and b^* as well as an optimal alignment between $\ddot{\theta}_N$ and the subsequence $\ddot{\theta}_T\,(a^*: b^*)$ can be computed by a modification in the initialization of the DTW algorithm as described in Section 3.4.1.

The basic idea is not to penalize the omissions in the alignment between X and Y that appear at the beginning and at the end of $\ddot{\theta}_N$. More precisely, we modify the definition of the accumulated cost matrix D as

$$\text{First Row: } D\,(1, j) = \sum_{k=1}^{j} c\,(x_1, y_j)\,, j \in [1: M] \tag{12}$$

$$\text{First column: } D(i,1) \;=\; \sum_{k=1}^{i} c\,(x_i, y_1)\,, i \;\in\; [1{:}\,N] \tag{13}$$

In order to detect trip with elastic time series dynamic alignment properties, the DTW algorithm was integrated into the trip detection algorithm and the flow process of its operation is described as follow.

Figure 22

Mean and Two-Standard Deviation (2σ) Envelope of the Difference Between Two Full Gait Cycle Lower Back Angular Acceleration Signals During Normal Walking

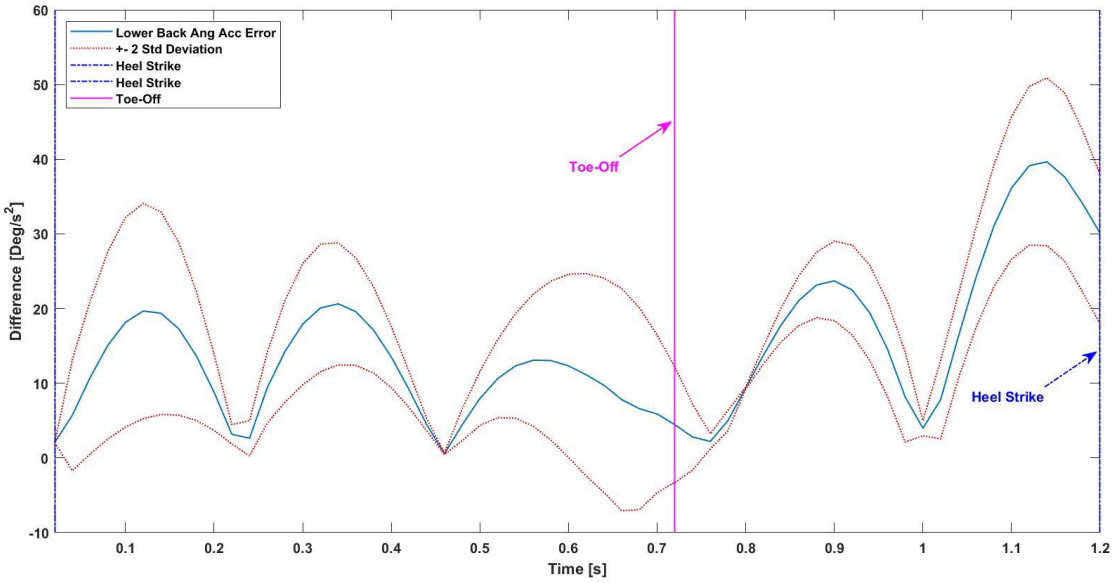

Note. The mean (blue) lower back angular acceleration warped signal difference using DTW of ten trials during normal walking with a two standard deviation envelope (red) and marked toe-off instance (magenta).

Figure 23

Decision Tree of the Trip Detection Algorithm Using the DTW

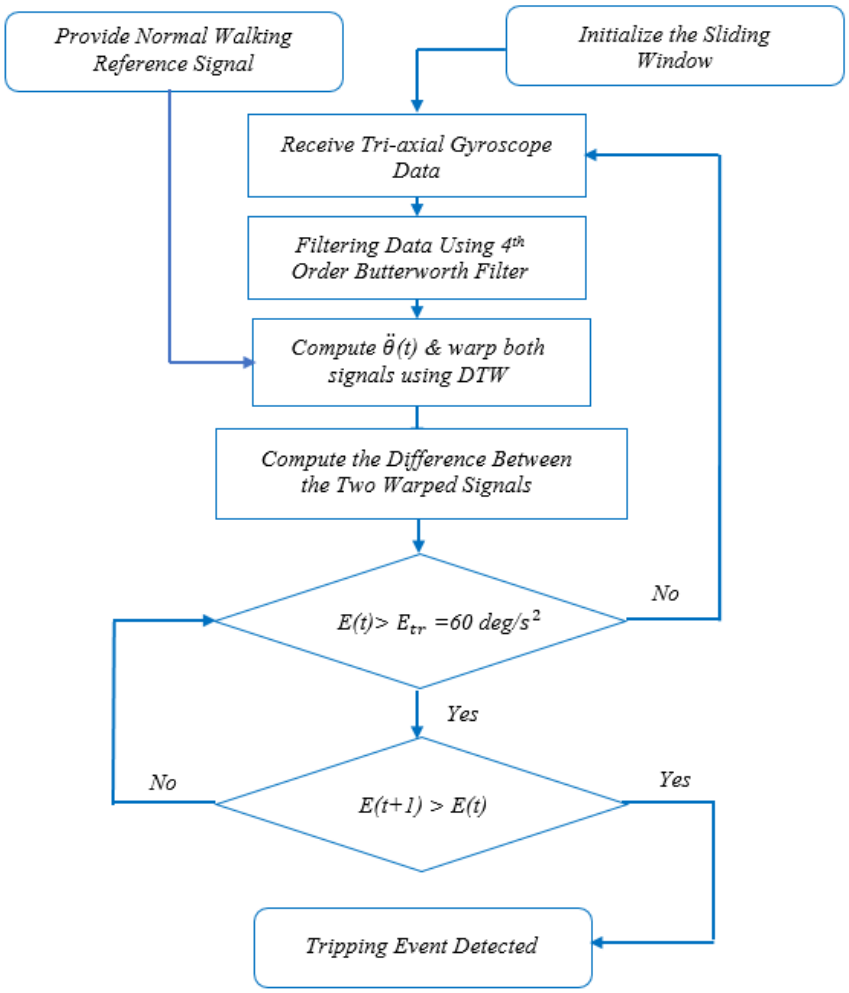

Note. Trip is detected if the difference between the warped reference signal and the testing signal exceeds the (2σ) threshold and keeps increasing in the next instance.

The first step consists of the initialization process by defining the width and type of the sliding window of the input data as well as introducing a data of full normal walking gait cycle (i.e., length of data between two consecutive heel strikes) used as the main reference for signal comparison. In the next step, the raw data from the IMU

sensors are filtered to eliminate any instrumentation noise in the measurements that can affect the calculated cost function. Next, the local distances c between the two signals are calculated, the confusion matrix is constructed, and the optimal path is determined using the DTW to provide the best alignment between both signals.

Lastly, a fixed threshold (E_{tr}) is introduced to provide a reference value as a criterion to determine trip onset. The criteria that is used to differentiate between the trip and non-trip situation was determined based on computing the difference between two full normal walking signals after being warped in time using the proposed algorithm.

The normal walking signals were extracted from ten total trials obtained experimentally from two participants and both the mean and standard deviation of the difference between the different warped signals were computed, as shown in Figure 22.

The threshold value was determined as the maximum difference value E between the mean and the bounds of the two-standard deviation (2σ) envelope of the normal walking signals after being warped using DTW. Trip was detected in trials when the computed difference E between the measured signals after being warped and aligned surpassed the threshold value of E_{tr} =60 deg/s^2.

To provide a better understanding of the algorithm, Figure 23 shows a visualization of the decision tree of the detection algorithm using DTW. In order to provide an insight about the warping effect of DTW on two signals being compared to each other, Figure 24 shows comparison plots of signal with and without applied DTW.

Figure 24

Normal and Early Trip Trial Comparison with and without the Use of DTW

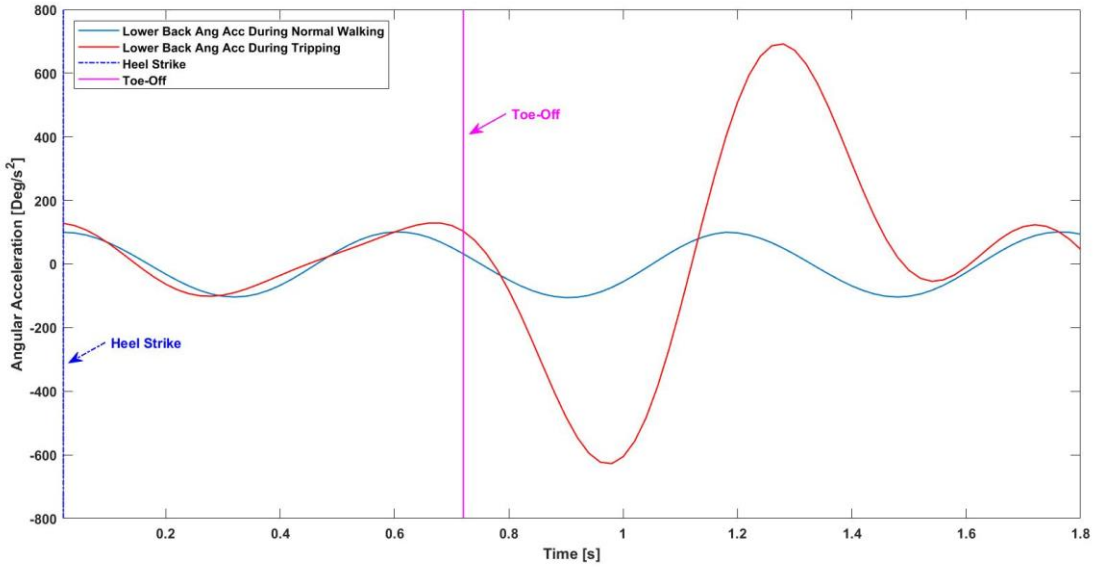

A

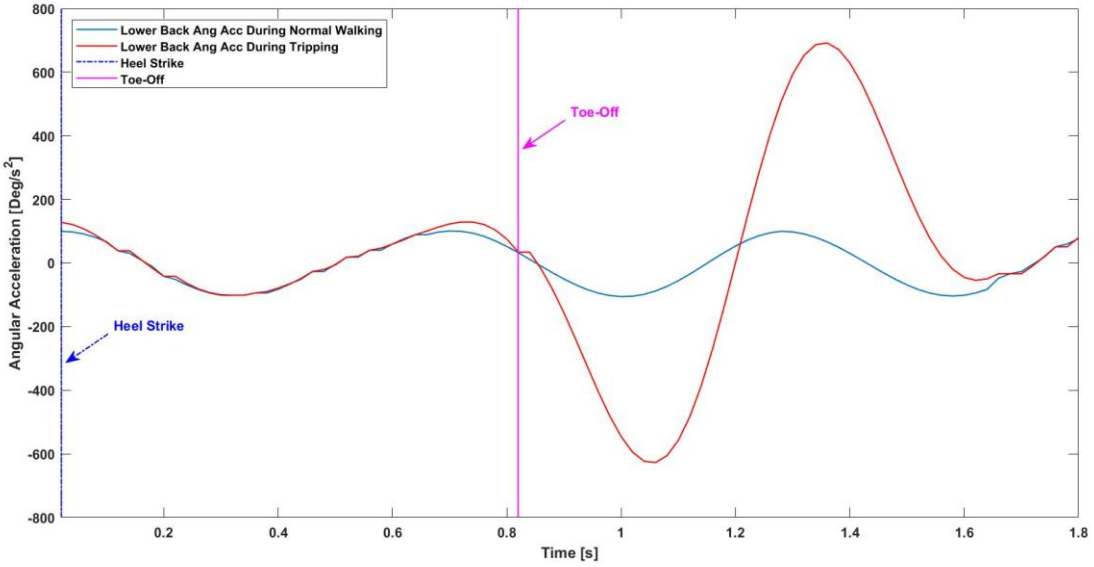

B

Note. Normal walking and tripping signal A, without and B, with the application of DTW.

Figure 25

Lower Back Angular Acceleration Normal Walking with Respect to Tripping for the Case of Early and Mid-Trip Using DTW

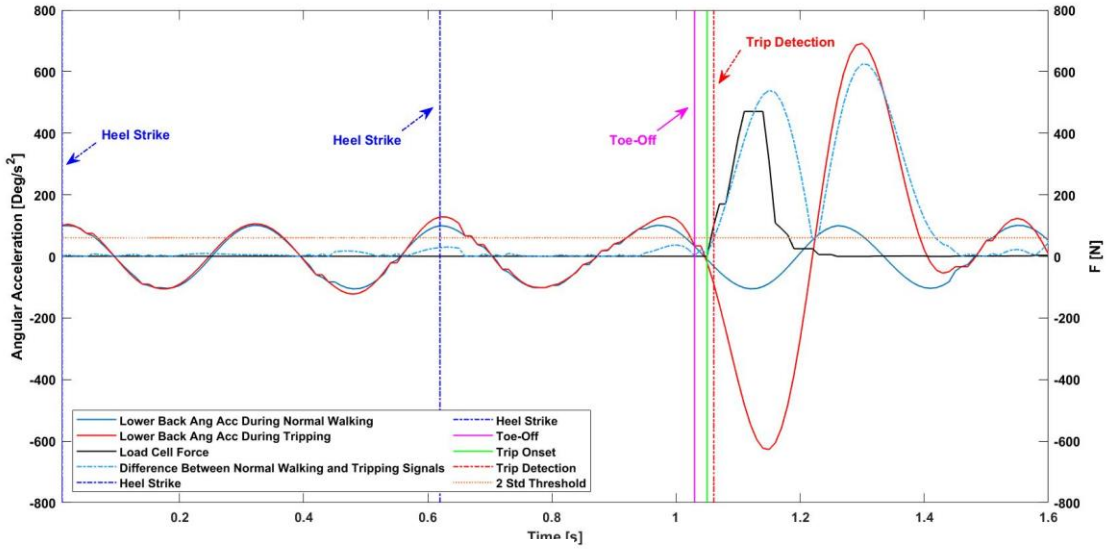

A

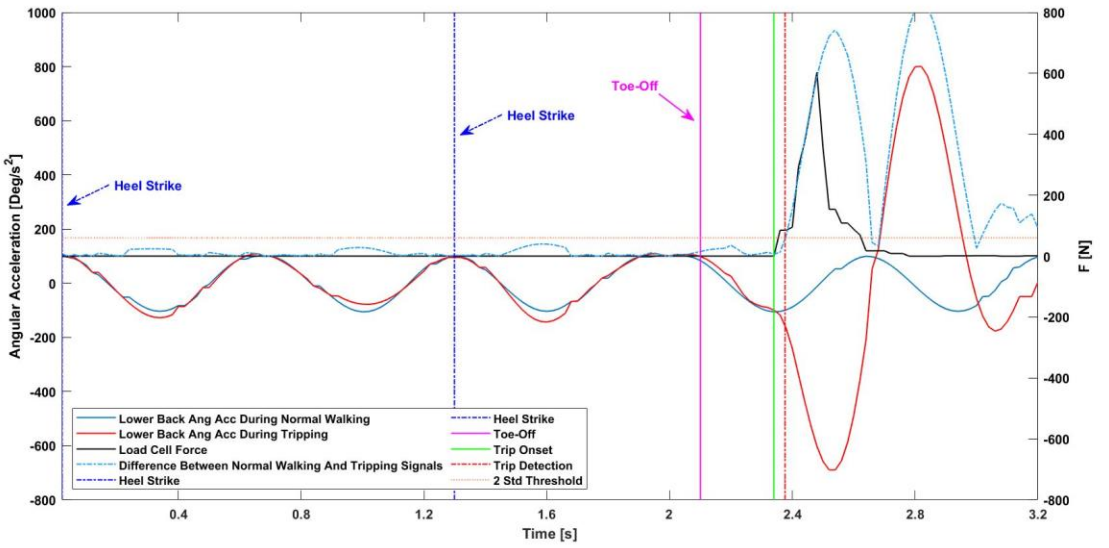

B

Note. Two full steps are provided in both plots with one being normal walking and one including trip disturbance. A, Early trip case with trip detection time 26ms. B, Mid-trip case with trip detection time of 39ms.

Figure 26

Lower Back Angular Acceleration Normal Walking with Respect to Tripping for the Case of Late Trip Using DTW

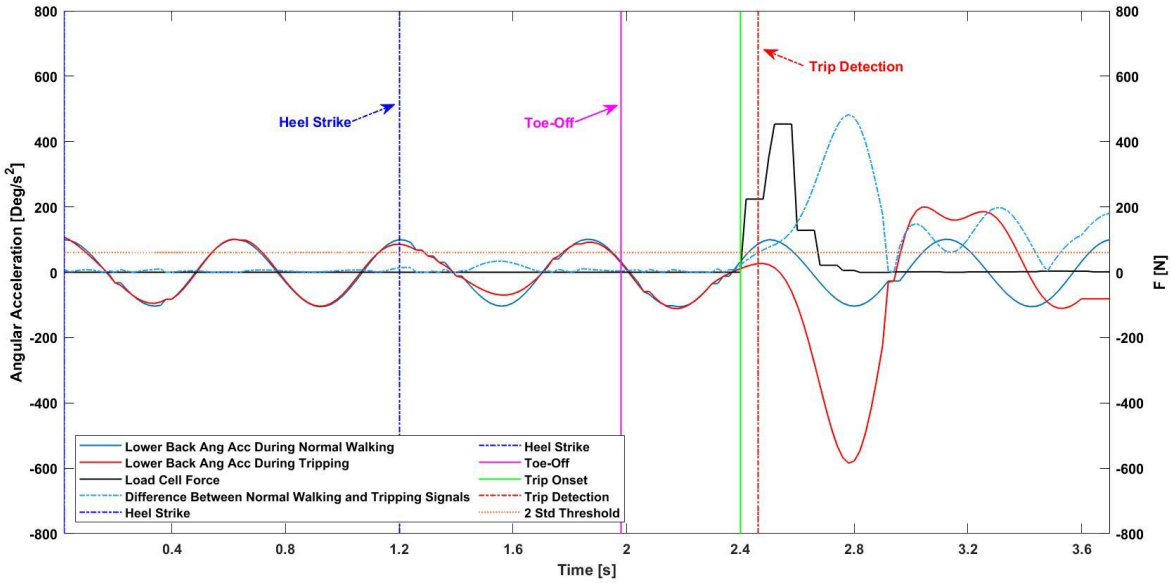

Note. Two full steps are provided in the plot with one being normal walking and the other being a late trip with trip detection time 42 ms.

Specifically, the angular acceleration profiles of normal walking and trip's warped (Fig. 24 (A)) and non-warped (Fig. 24 (B) signals of different lengths compared to the normal walking are shown to demonstrate the difference after signal warping.

Comparison results of non-warped and warped signals show that during the stance phase both signals are similar but no perfect alignment exist due to walking gait variations, differences in walking speed, and possible measurement or instrument errors.

Figure 27

Cost Matrix with Minimum Cost Warp Path Used for Alignment for the Case of Early and Mid-Trip

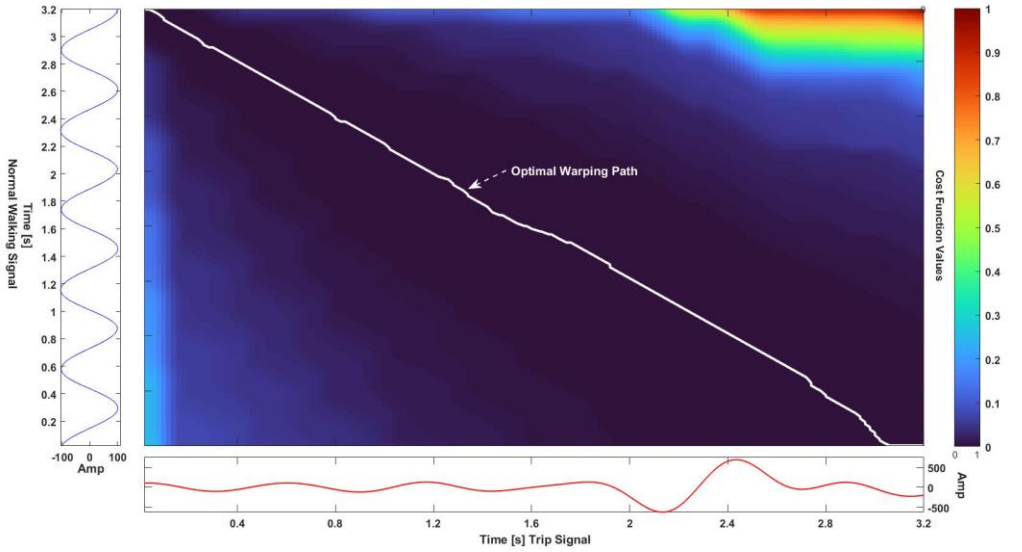

A

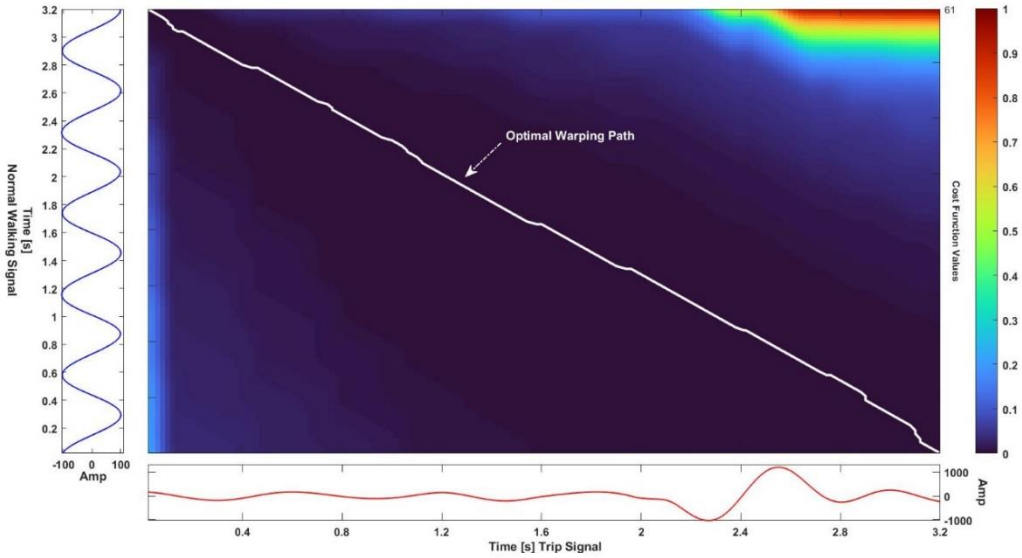

B

Note. The confusion matrix with optimal warping path used to align trip and normal walking signals for A, early and B, mid-trip trial. The encircled regions show the effect of trip perturbation

Thus, its direct calculation of the difference between the reference normal walking and trip signal will not provide accurate results, since the Euclidian distance calculation will not reflect their actual similarity.

Applying the DTW can significantly minimize or eliminate these differences. To demonstrate the effectiveness of the proposed DTW-based trip detection algorithm in terms trip detection time and detection rate, we analyzed all 30 trip trials. Figure 25 and 26 shows results of the representative trials of early, mid, and late trips being warped in time with respect to a reference signal of normal walking.

The results show that the resultant difference between both signals after being warped using DTW during the normal walking phase (i.e., portion before labeled toe-off event) lays under the two-standard deviation threshold with its values being close to zero. This result indicate that both the reference and tripping signal follow the same harmonic trend. When the trip occurs, the value of the resultant difference increases dramatically and surpasses the threshold, hence trip is detected.

For the purpose of clarification of the way the optimal path is selected by the algorithm during alignment of both the normal walking and trip signal, Figures 27 and Figure 28 show plots of the cost matrix values with the selected minimum cost warping path for the early, mid, and late trips.

Each pixel in the confusion matrix presents a cost value with a range between 0 (blue) and 1 (red). Higher values (brighter colors) present cells with high cost which implicate larger difference between both signals' points, while lower values (dark colors) implicate low cost values, which means a high similarity between both points. Figure 29

shows a histogram of the average and standard deviation values of trip detection times for early, mid and late trip across the entire data set of 30 trials for both participants.

Figure 28

Cost Matrix with Minimum Cost Warp Path Used for Alignment for the Case of Late Trip

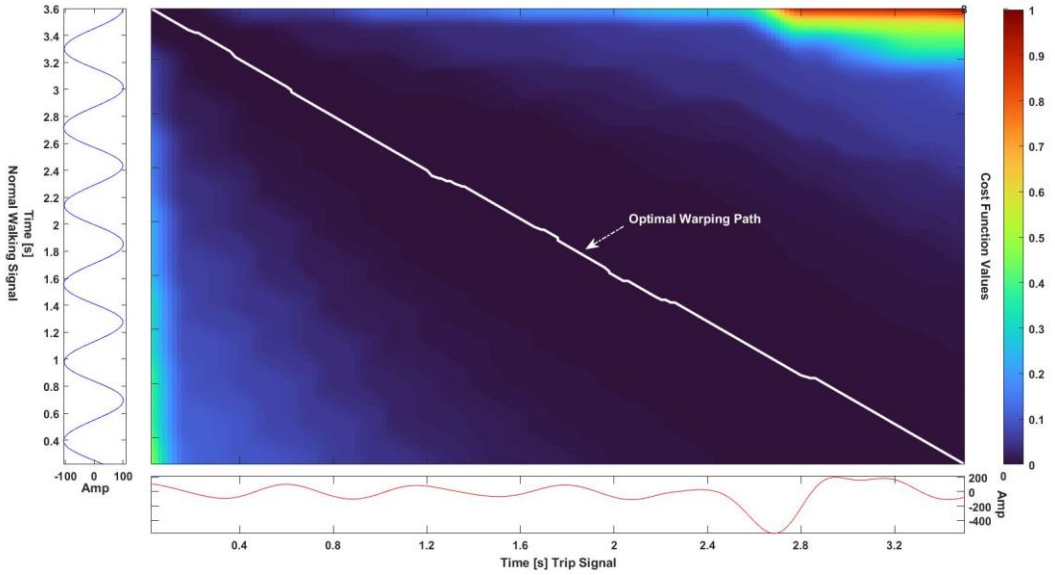

Note. The confusion matrix with optimal warping path used to align trip and normal walking signals for late trip trial. The encircled regions show the effect of trip perturbation.

The results show that the DTW algorithm can rapidly detect different types of trips effectively with an overall mean detection time of 70 ms and a detection rate of 100% across the early, mid and late trips with different perturbation duration lengths (50-200 ms).

The DTW capabilities of comparing signals that have different lengths or phase with respect to time and allowing real-time signal comparison makes this method an attractive approach to rapidly detect trips.

Figure 29

Comparison of the Trip Detection Times (Mean and Standard Deviation) Across Both Subjects for the DTW Algorithm

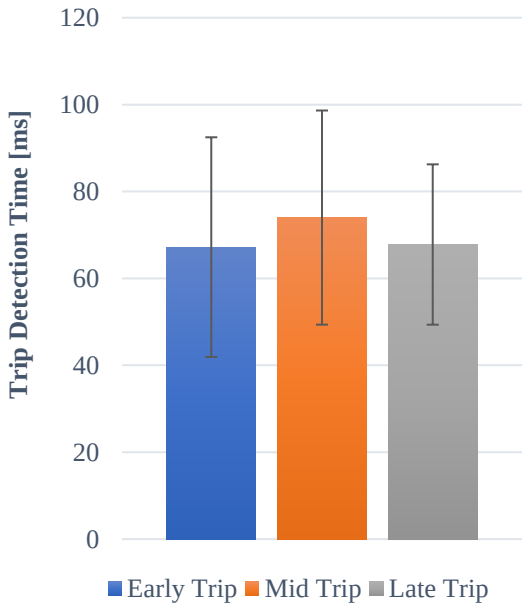

Note. Between both subjects and for the early, mid and late trip the biggest observed mean value was 74 ms while the smallest was 67.2 ms.

In conclusion, this chapter presents different time domain-based methods for rapid trip detections using signals from body-worn inertial sensors. The average detection times from all methods are several times shorter compared to the human voluntary reactions.

In the first portion of this chapter, three algorithms using fixed thresholds were developed based on the lower trunk angular jerk, signal magnitude area of the lower back angular acceleration, and the RMS of the lower back angular acceleration.

The second part of this chapter presents trip detection method using the integration of an elastic time domain used for signal alignments. Overall, both the jerk and the quadratic mean methods showed the best results in detecting trip with the fattest mean detection times across all the trials of 43ms and 51ms, respectively.

These rapid detection times are primarily possible due to the fact that RMS amplifies the abrupt changes in the mean values of the acceleration within the sliding window, while the jerk shows the rate of the lower back acceleration that is sensitive to a sudden trunk movement during trip perturbation.

The simple but effective RMS and jerk algorithms are suitable for real time implementation specially as they require only simple calculations and do not require high computational power to work efficiently. However, both methods in addition to the SMA-based trip detection method suffer from the problematics related to the static threshold implementation as the main source of decision.

The fixed threshold-based methods are not flexible in regards to the variations in walking speed or cadency of the gait that also motivated this work to provide more flexible detections algorithms such as DTW. The performance of the DTW-based trip detection algorithm was slightly inferior compared to the developed jerk- or RMS-based algorithms with a mean detection time of 70 ms.

However, it provides more flexibility in trip detection as it can accommodate the changes in walking speed, variation of gait cadency, and can handle difference in phase shift of signals with great efficiently. Indeed, the DTW algorithm is more complex and requires larger computational power compared to other methods.

Chapter 4

Frequency-Based Trip Detection Method

In this chapter, a frequency decomposition-based trip detection algorithm using a lower back angular acceleration signal ($\ddot{\theta}$) in the sagittal plane is described. The developed algorithm is based on the continuous wavelet transform (CWT) using a custom-designed reference signal called mother wavelet. The lower back angular acceleration ($\ddot{\theta}$) in the sagittal plane was obtained by direct integration of the angular velocity measured by the IMU system. The proposed approach allows to break up the recoded trip signal into shifted and scaled version of the predefined mother wavelet sample that is constructed based on the mean signal of multiple trip events. The continuous signal of ($\ddot{\theta}$) is then compared to the generated mother wavelet to identify the trip perturbation onset. Trip was detected when the correlation coefficient of the measured signal surpassed the fixed threshold value CWT_{tr}.Threshold was defined as the maximum value of the two-standard deviation (2σ) envelope obtained from the correlation coefficient of normal walking trials of subjects after being treated by the CWT.

4.1. Continuous Wavelet Transform

Methods discussed in Chapter 3 all use the temporal domain-based techniques to detect trip event and were shown to be efficient. However, signal analysis in time domain does not always reveal complete information included in a signal and therefore, a frequency analysis of a trip signal can provide additional and critical information about

trip occurrence that is not observable using only time domain methods. The most well-known frequency analysis tool, which is the Fourier analysis, has been used for years effectively in order to provide comprehensive signal analysis in frequency domain. Unfortunately, the Fourier analysis is not suitable to be directly used for our trip detection purpose, since during the signal transformation in to the frequency domain, the time information is lost.

In other words, when a Fourier transform analysis of a trip signal is performed, it is impossible to identify when a particular perturbation event occurred. Therefore, there is a need to use an alternative frequency analysis method such as the continuous wavelet transform (CWT) that can correlate the time domain information with the frequency domain.

A continuous wavelet transform is a mathematical frequency decomposition tool that converts a signal into a different form by allowing scaling and translation of a base or mother wavelets to vary continuously. A mother wavelet is a reference signal wave defined on a short interval and constrained by specific conditions. The signal has to have an oscillating wavelike behavior with its energy concentrated in time domain. This wavelet reference is needed in order to accomplish the scaling and the translations required to perform the continuous wavelet transformation. Signal comparison of $\ddot{\theta}$ to the mother wavelet through CWT allows to reveal features and characteristics included in the original signal before decomposition.

Let $\ddot{\theta}_T$ and ψ of respective lengths N and M be the input signal of lower back angular acceleration and the mother wavelet reference tripping signal, respectively. Using

our trip-based mother wavelet, the similarity between both signals can be described by computing the sliding cross-correlation coefficient defined as

$$\gamma(\mathrm{a},\tau) = \int \ddot{\theta}_T(t)\bar{\psi}_{a,\tau}(t)dt, \tag{14}$$

Where $\bar{\psi}_{a,\tau}$. present the complex conjugate of $\psi_{a,\tau}$. The above equation can provide an insight about how a function $\ddot{\theta}_T(\mathrm{t})$ is decomposed into a set of different mother wavelet versions $\psi_{a,\tau}$ .The variables *a* and τ presents the new dimensions of the transformation with (a) being the scale and τ being the translation, after the wavelet transform. For completeness of the process from a mathematical point of view, the inverse wavelet transform can be obtained using the following expression

$$\ddot{\theta}_T(t) = \iint \gamma(\mathrm{a},\tau)\,\psi_{a,\tau}(t)d\tau da \tag{15}$$

All sub-wavelets also called as daughter wavelets are generated based on the scaling and translation of mother wavelet $\psi_{a,\tau}$. The mother wavelet is defined as

$$\psi_{a,\tau}(t) = \frac{1}{\sqrt{a}}\,\psi\left(\frac{(t-\tau)}{a}\right) \tag{16}$$

The purpose of term $(\frac{1}{\sqrt{a}})$ in the mother-wavelet is to provide energy normalization across different scales and to ensure that $\|\psi_{a,\tau}(t)\|$ is independent of variables *a* and τ. It is important to notice that in the equations (16) above, no specific definition for the wavelet type was made, which is the main difference between the wavelet transform and the Fourier or other similar transforms.

It is also worth noticing that the wavelet transforms theories deal with general properties of wavelet without any specificity as long as the wavelet respects the main wavelet property conditions, which is the admissibility condition. The admissibility condition of a mother wavelet can be expressed mathematically as

$$\int \frac{|\Psi(\omega)|^2}{|\omega|}\, d\omega < +\infty, \tag{17}$$

where Ψ(ω) presents the Fourier transform of ψ(t). The implication of this condition is that the integrable squared function ψ(t).

that satisfies the described mathematical relationship can be used to analyze and reconstruct the signal without any loss of information during the process. In addition, the condition implies that the Fourier transform of the mother wavelet function ψ(t) is zero at a zero frequency, which is expressed as $|\Psi(\omega)|^2$=0 at ω=0.

Another implication from the previous relationship is that at frequency ω=0, the average value of the wavelet in the time domain is equal to zero that is expressed in a mathematical presentation as $\int \psi(t)dt$=0. If the average value of the wavelet is zero in the time domain that implicates that the signal ψ(t) needs to be oscillatory or in other words, the function ψ(t) must be a wave. In addition, we can conclude that the wavelet transforms of one-dimensional function is two-dimensional since both scaling and translation are added.

4.1.1. *Scale Tuning and Selection*

As described in previous section, continuous wavelet transforms use two main properties to make the needed frequency decomposition, which are scaling and shifting of the mother wavelet signal. Scaling presents how much the wavelet is compressed or stretched in time domain.

The smaller the scale factor, the more wavelet is compressed and the higher the frequency of a targeted mother signal, which implies the rapidly changing signal that can include features of rapid anomalies in a signal (e.g., trip) that can be detected with higher resolution.

On the other hand, the bigger the scale factor, the lower is the frequency and the more stretched is the wavelet. Such mother wavelet configuration allows for comparison and effective detection of slowly changing features in a signal. A relationship that correlates the scale factor (a) is defined as

$$a = \frac{Fc}{Fa\ Fs}, \tag{18}$$

where Fa is the frequency corresponding to the scale, Fs is the sampling frequency, and Fc is the central frequency of the mother wavelet being used. Thus, it is important to carefully select the scale factor for optimal detection of trip perturbation.

In order to select the appropriate scale for the trip signal analysis, a short Fourier transform was applied on all recorded trials obtained during the experiments to examine the most common range of frequencies during normal walking and trips triggered at

different instances. Figure 30 shows the Fourier analysis results of the lower back angular acceleration $\ddot{\theta}$ signal of the representative early, mid, late trip trials. The most common frequencies observed during normal walking and trip gaits across various walking speeds were in a range between 1-4 Hz, with the majority of the frequency changes located at the 2 Hz range.

Figure 30

Frequency Analysis of Normal Walking, Early, Mid and Late Trips Using Fast Fourier Transform

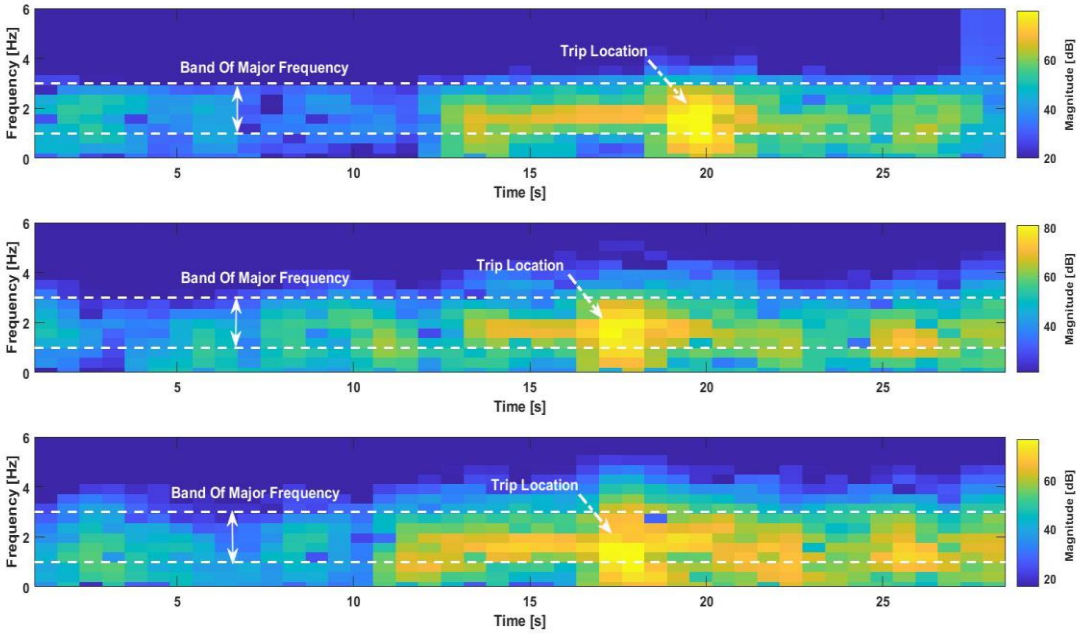

Note. Results of the frequency analysis of the lower back angular acceleration $\ddot{\theta}$ signal across the entire duration of three representative trials indicate the most common frequency range being 1-4 Hz. Each trial contains several normal walking steps and trip perturbed gait with (A) early, (B) mid, and (C) late trip onset.

This observation is in accordance with the biomechanics literature, where the frequency of human motion during walking is reported to be ~2 Hz [86]. Therefore, in our analysis we considered the corresponding frequency equivalent scale of a= 50.

4.1.2. *Mother Wavelet Design and Integration Based on Trip Data*

Human trip perturbation results in a loss of balance event due to the shifting of the center of gravity around the foot contact point, which causes the trunk to rotate forward and pivot around that point. Therefore, the lower back angular acceleration signal $\ddot{\theta}$ during trip phase increases compared to the signal observed during walking.

In Chapter 2, such signal behavior was exploited in order to detect gait perturbation, which is different compared to the main approach in this chapter, where the lower back angular acceleration signal $\ddot{\theta}$ is used to design a mother wavelet signal based on trip perturbation patterns.

The wavelet is designed by averaging 30 trip trials with trip onsets at different swing phase portions and with different durations that were collected during our experimental trials. Figure 31 shows the mean profile of the trials. The degree of similarity between the continuously measured signal $\ddot{\theta}$ is compared to the mother-wavelet through wavelet analysis to detect trip events.

The process of designing the mother wavelet starts by using a 2 second window of the average signal of the trip perturbation portion with the trip onset being at its center. The treatment of centering trip onset timing is intentional to allow a recognition of the trip signal characteristic features as soon as the perturbation starts.

The obtained average trip signal was transformed into an adapted mother wavelet using a least-squares polynomial approximation and defined on the interval [0,1], with the admissibility condition related to the wavelet definition being satisfied. Figure 32 shows obtained result of the mother wavelet trip signal.

Figure 31

Averaged Lower Back Angular Acceleration Signal $\ddot{\theta}$ During Trip Perturbation with Its Two-Standard Deviation (σ) Envelope

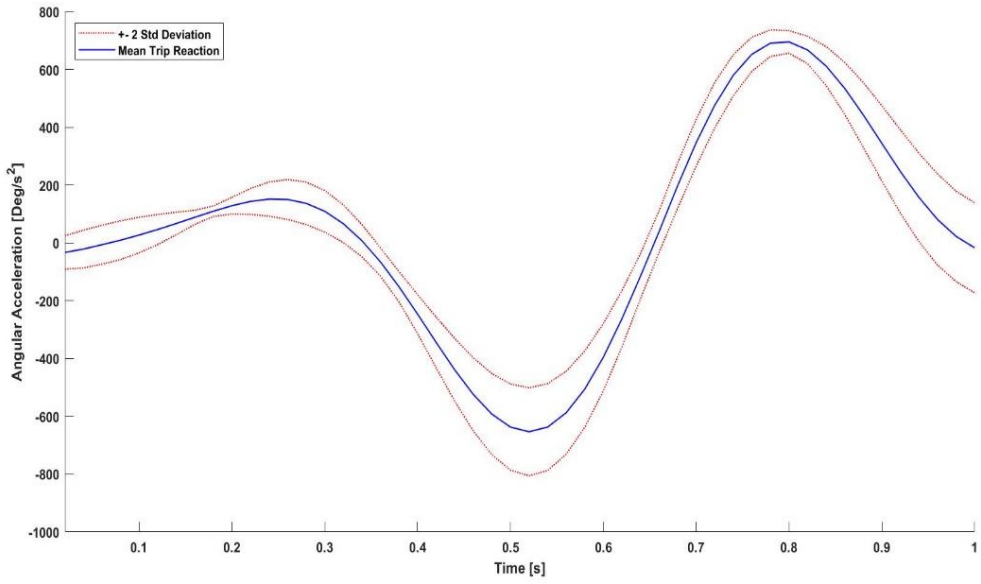

Note. The obtained mean trip pattern curve has a 1 second window width and was obtained using 30 different trip perturbation patterns.

After the adapted mother wavelet is constructed, the next step is to integrate it in the trip detection algorithm and inspect the performance of the algorithm on different trip perturbation signals.

The first step of the algorithm starts with the initialization process of selecting the width and the type of the sliding window used to feed the measurements into the algorithm. In the next step, the raw measurement data coming from the IMU sensors are filtered using 2th order Butterworth filter with a 6 Hz cutoff frequency.

Figure 32

Normalized and Transformed Averaged Trip Signal with Its Adapted Mother Wavelet

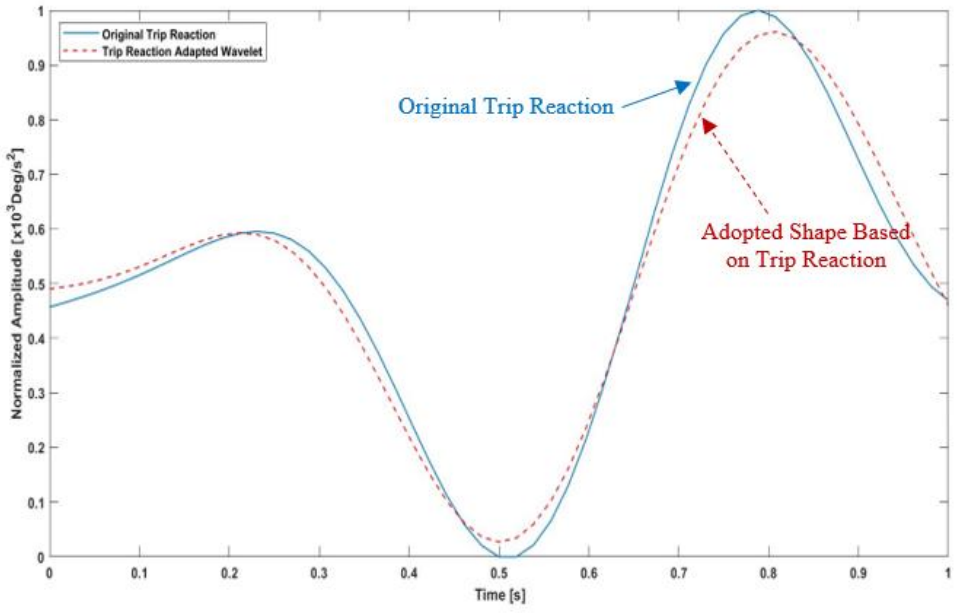

Note. The obtained adapted mother wavelet curve (dashed red) is normalized in the [0 1] interval generated from 2 second actual trip pattern.

The pre-defined, normalized, adopted mother wavelet is then used in the CWT algorithm to perform the scaling and shifting operations using the mother wavelet as a main reference that allows to compare signal similarities and detect various trip types.

Figure 33

Mean Lower Back Angular Acceleration Correlation Coefficient During Normal Walking After the Use of CWT with Two-Standard Deviation (2σ) Envelope

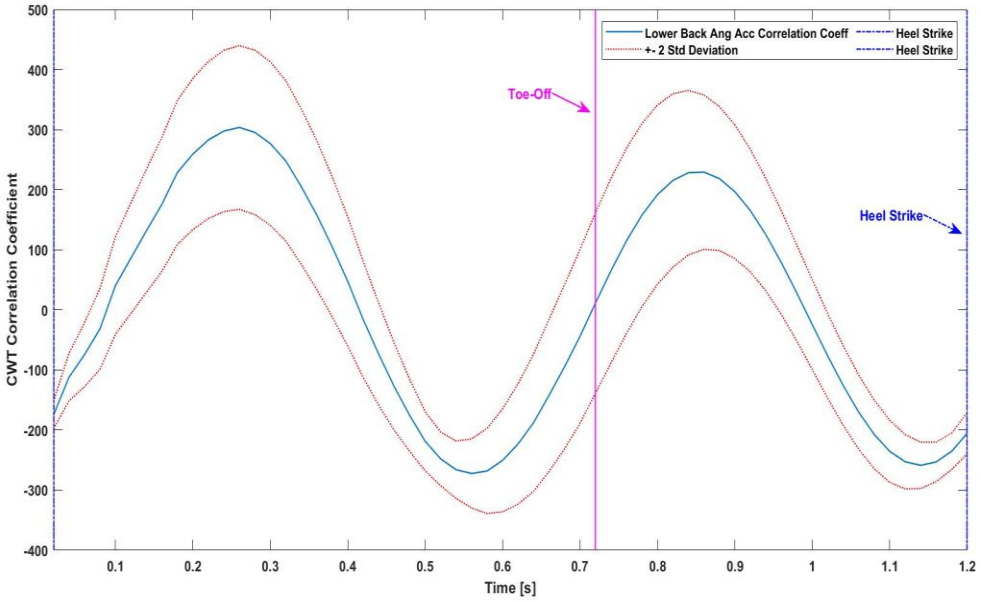

Note. The mean of lower back angular acceleration correlation coefficient signals of ten trials during normal walking after applying the CWT is presented in blue color with its two standard deviation envelope and toe-off instance in dashed red and magenta colors, respectively.

Figure 34

Trip Detection Decision Tree Algorithm Based on the Continuous Wavelet Transform

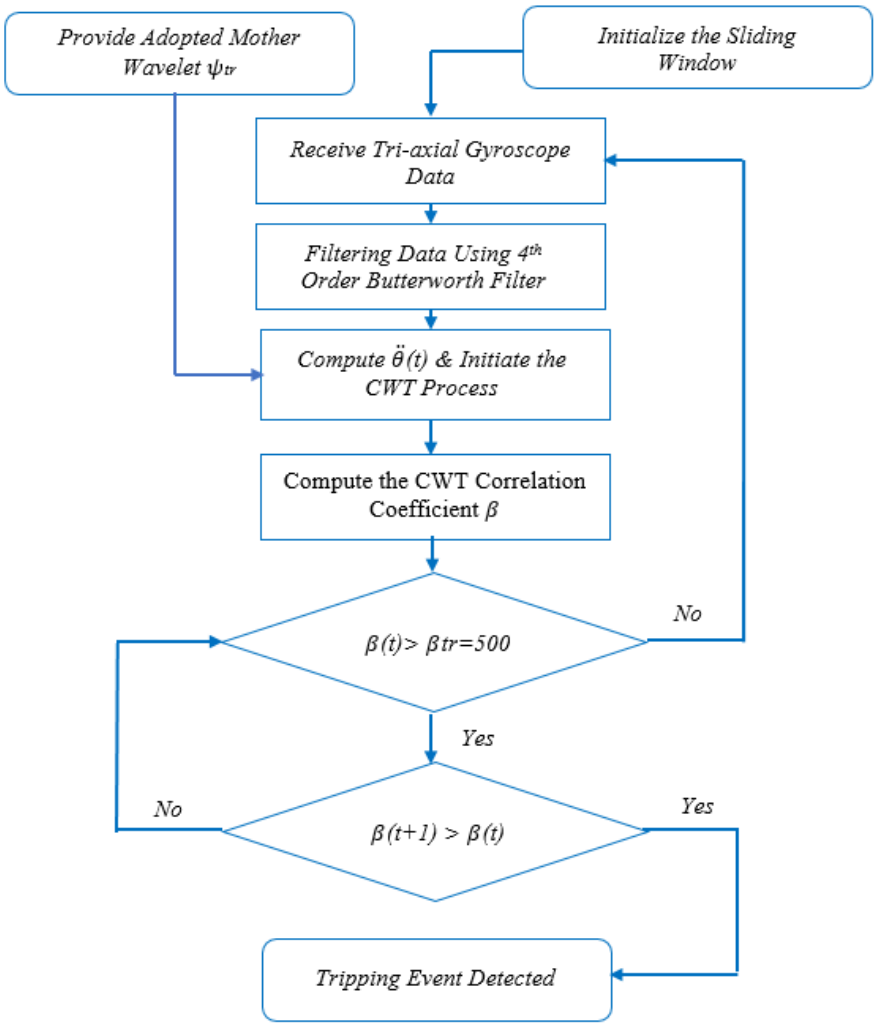

Note. The trip event is detected if CWT correlation coefficient exceeds the two-standard deviation threshold and keep getting bigger in the next instance.

The continuous wavelet transform correlation coefficient are calculated and compared to a fixed threshold values to indicate trip onset when the coefficient values exceed the threshold value.

Figure 35

CWT Correlation Coefficient Between the Lower Back Angular Acceleration During Normal Walking and Tripping and the Mother-Wavelet for the Case of Early Trip

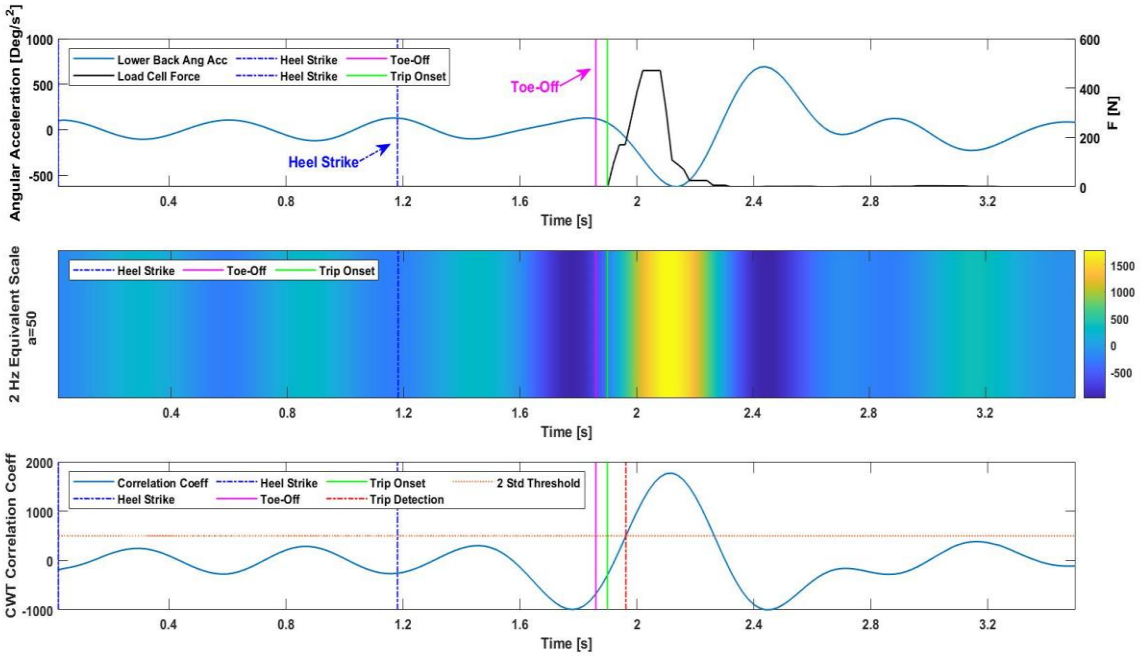

Note. Plots show results of two full steps. The first step represents normal walking and the second one includes trip event. A, Profile of lower back angular acceleration during normal walking and early tripping event. B, Results of trip detection using equivalent frequency scale of 2 Hz (a = 50) for trip detection. C, CWT correlation coefficient between mother wavelet and the trip signal $\ddot{\theta}$ for the case of early trip with trip detection time of 62 ms.

The threshold was taken as the maximum value of the two-standard deviation (2σ) envelope obtained from the CWT correlation coefficient between the mother wavelet and ten normal walking trials from two subjects as shown in Figure 33. The trip detection decision tree of the proposed CWT-based algorithm is presented in Figure 34. Figures 35, 36, and 37 present three representative trip trials that include one normal walking gait followed by trip occurrence during an early, mid and late swing portion gait cycle. The frequency equivalent scale with its resemblance coefficient is demonstrated for each trial in addition to the correlation coefficient between the mother wavelet and the tested trial.

From the continuous wavelet analysis of the trial that includes both normal walking and early trip, we can observe that during normal walking (< 1.8 sec), the values of the correlation coefficient are low (<500), which indicate low signal similarity. As soon as trip is induced, the value of the similarity coefficient increases (manifested by brighter color in Figure 35 (B)) and the spike in the correlation coefficient indicates the presence of a trip perturbation based on the comparison to the mother wavelet.

Figure 35 (A) also shows measurements from the load cell of induced force to the foot and its duration that trigger trip that are used for comparison and validation of the purposed trip detection algorithm. Figures 36 and 37 shows results of trip detection algorithm from a representative subject for trips triggered during mid and late swing phase, respectively. The detection times of mid and late trip were 81 ms and 80 ms, respectively, indicating consistent performance of the CWT-based trip detection algorithm. It is important to realize that for different scales, the detection time can increase or decrease depending on the frequency used.

Figure 36

CWT Correlation Coefficient Between the Lower Back Angular Acceleration During Normal Walking and Tripping and the Mother-Wavelet for the Case of Mid-Trip

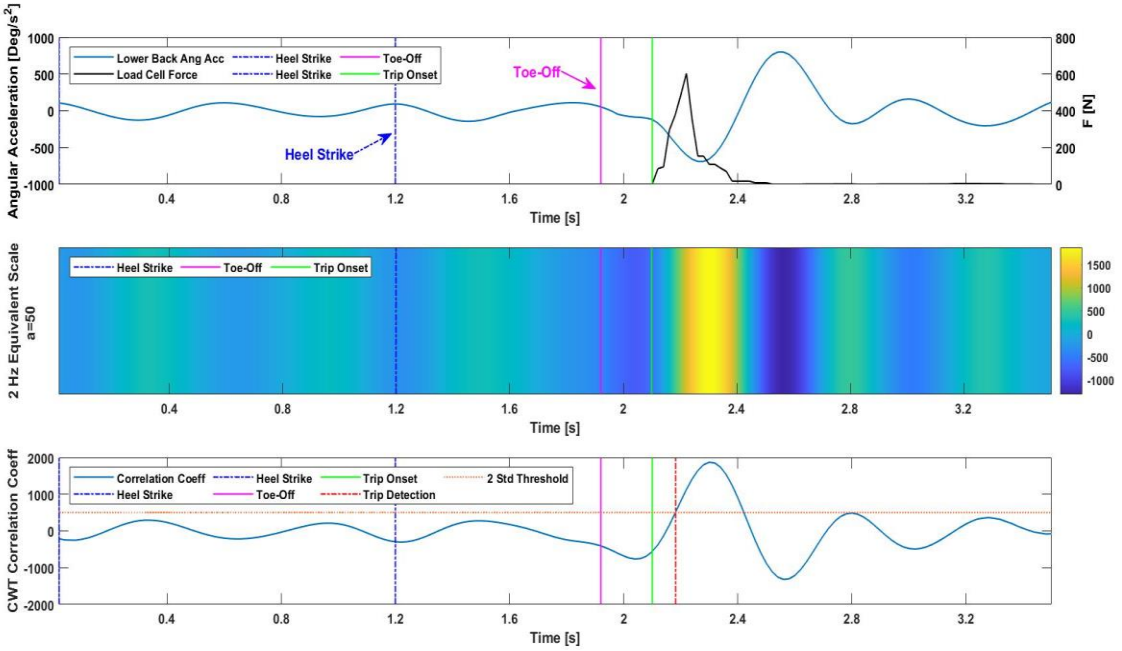

Note. Plots show two full steps. The first step represents normal walking and the second one includes trip event. A, Profile of lower back angular acceleration during normal walking and early tripping event. B, Results of trip detection using equivalent frequency scale of 2 Hz (a = 50) for trip detection. C, CWT correlation coefficient between mother wavelet and the trip signal $\ddot{\theta}$ for the case of early trip with trip detection time of 81 ms.

As a general guide, the smaller the scale, the higher detection resolution is with respect to small abrupt changes in the signal (zoom in in terms of frequency analysis) and slow changes in signal are detected more poorly due to the small shifting of the mother wavelet.

Figure 37

CWT Correlation Coefficient Between the Lower Back Angular Acceleration During Normal Walking and Tripping and the Mother-Wavelet for the Case of Late Trip

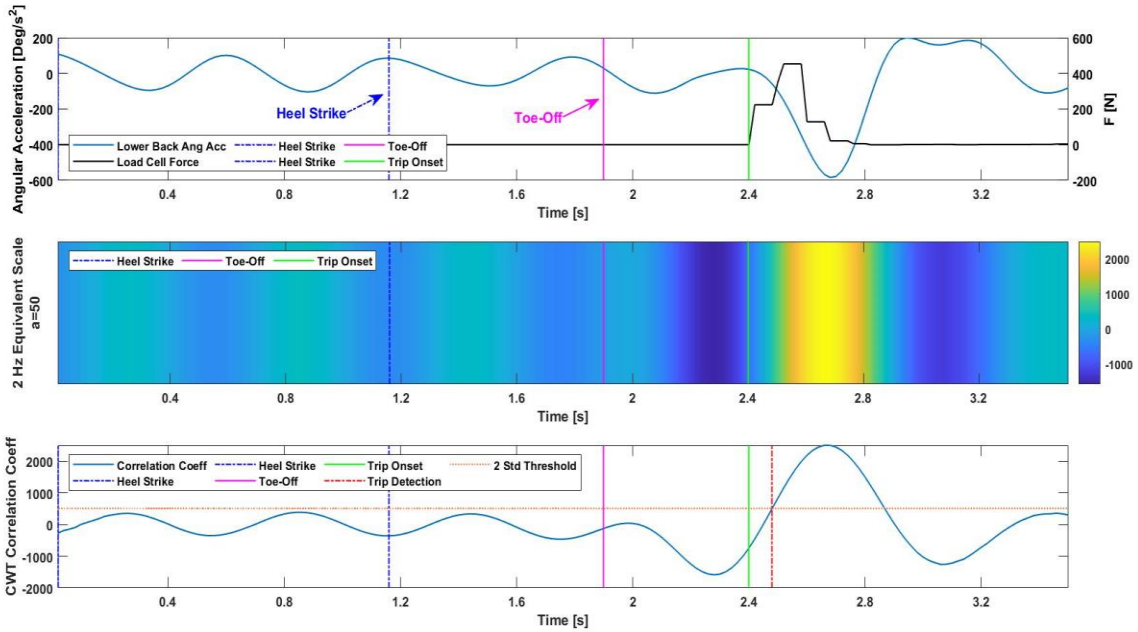

Note. Plots show results of two full steps. The first step represents normal walking and the second one includes trip event. A, Profile of lower back angular acceleration during normal walking and early tripping event. B, Results of trip detection using equivalent frequency scale of 2 Hz (a = 50) for trip detection. C, CWT correlation coefficient between mother wavelet and the trip signal $\ddot{\theta}$ for the case of early trip with trip detection time of 80 ms

Therefore, the selection of the scale needs to be carefully considered since the selection changes based on the needed objective. It is worth to mention that the plot presenting the trip detection at the scaling frequency provides the information at a

frequency levels, while for the plot presenting correlation coefficient it presents the result of the correlation operation between the mother wavelet and the tripping signal.

Figure 38

Comparison of the Trip Detection Times (Mean and Standard Deviation) Across Both Subjects for the CWT Algorithm

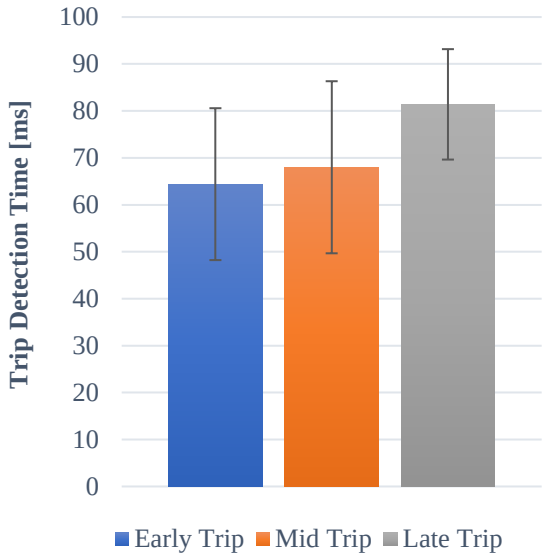

Note. Between both subjects and for the early, mid and late trip the biggest observed mean value was 81.4 ms while the smallest was 64.6 ms.

Figure 38 shows results of trip detection time using CWT-based methods. The method successfully detected all early, mid, and late trips from both subjects with various trip perturbation duration (50 – 150 ms).

The results show that the CWT algorithm can distinguish between trips and non-trips case effectively with an overall mean trip detection time across all the trials of 71 ms and a detection rate of 100% for all different trip types of trips.

4.2. Planar Covariation Law

Methods discussed in this chapter so far allowed the detection of trip perturbation in a very short time, however, no quantification of the trip events with respect to the duration of the perturbation neither the influence of such factor on the severity of the trip was discussed. Therefore, there is a need for a method that can provide such information regardless of external factor such as walking speed and gait frequency cycle. Planar covariation law (PCL) is an intersegmental co-ordination kinematic law in the biomechanics field. [87] PCL relates the elevation angles of the lower limb segments (i.e., thigh, shank, and foot) of the human body with respect to each other in a consistent manner that preserve posture control and locomotion by assuring maintenance of the dynamic equilibrium of the body during different tasks [87]. The elevation angles are defined as the absolute angles of the body segment link from the vertical axis.

Based on PCL law, different elevation angles of lower limbs during locomotion and its orientation should covary systematically with respect to each other to describe a closed loop on a plain in the 3D elevation angle space of an individual leg, which indicate a harmony between all three lower limbs joints and maintained status of dynamic equilibrium regardless of the walking speed and the gait cycle [88].

Therefore, the PCL law can be used to not only identify trip events, but also to correlate the duration of the perturbation with the severity of the trip by exploiting such kinematic rule.

Figure 39

Coplanar Variation Law of Elevating Angles of Thigh, Shank, and Thigh During Normal Walking and Different Trip Events

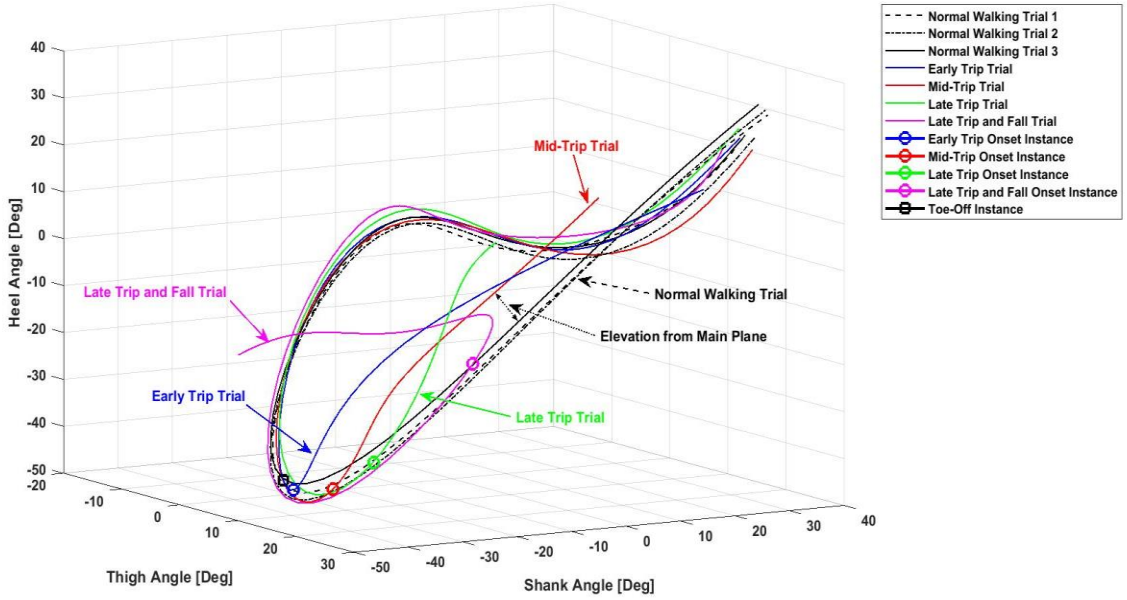

Note. Normal walking curves (black) lay in a plan with respect to the PCL law, while for different trip cases (blue, magenta, red, and green) the law is violated and the resultant curves deviate at an angle with respect to the main plain.

In order to inspect the validity of the PCL law and investigate the intersegmental co-ordination law and relationships during trip gait, all thirty trip trials were analyzed and compared. Relationships of different lower limb elevations angles of each participants' segments during the different trials were plotted with respect to each other to observe the difference during normal walking and trip gait. Figure 39 presents the planar covariation law of elevating angles of thigh, shank, and foot of a representative participant for three normal walking cycles and the early, mid, and late trip perturbations.

Results show that during normal walking the PCL law is well preserved and all the three elevating angles of the lower limbs interconnect with each other to form a closed loop pattern laying on a plane in a 3D space. Conversely, the trajectories representing trip trials start to deviate from this plane soon after the onset of trip perturbation. All three trip curves diverge from the normal walking plane and violate the law. Results in Figure 39 show that during trip perturbations, the resultant curves from lower limb segments elevating angles do not lay in the main plain ruled by the correlation of the different lower limb segments joints during locomotion and they deviate from it at an angle.

The angle is different for each shown trip trial and further analysis was performed to identify the relationship between the duration of the perturbation at which the movement of the perturbated leg is hindered and the angle of deviation of the trip trial plane ruled by the correlation of the different lower limb's elevation angles during trip event with respect to the PCL plan.

Thus, to further investigate this relationship, three trials of each trip perturbation category including early, mid and late trips that share almost the same perturbation onset but with different perturbation duration are plotted with respect to different normal walking trials behavior following the PCL law and the obtained results for the case of various early trips with different perturbation durations can be seen in Figure 40.

Figure 40

Coplanar Variation Law of Elevating Angles of Thigh, Shank and Thigh During Normal Walking and Early Trip Events with Different Perturbation Lengths

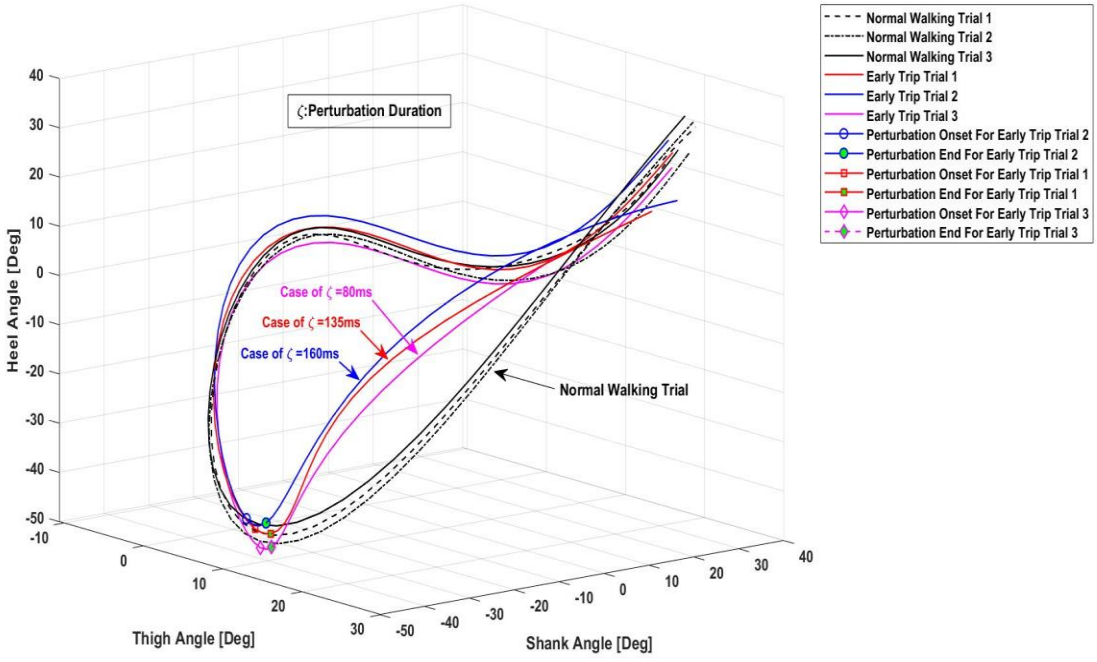

Note. Normal walking curves (blacks) lay in a plan with respect to the PCL law, while for different early trip cases (bleu, magenta and red) the law is violated and the resultant curves lay with an angle that increases with perturbation duration with respect to the main plan.

To further investigate this relationship, three trials of mid and late trips that share almost the same perturbation onset but with different perturbation duration are plotted for the case of mid-trips, the results for normal walking and different mid trips with different perturbation times with respect to the PCL normal walking plane in addition to moments of trip onset and trip perturbation end point are presented in Figure 41.

Figure 41

Coplanar Variation Law of Elevating Angles of Thigh, Shank and Thigh During Normal Walking and Mid-Trip Events with Different Perturbation Lengths

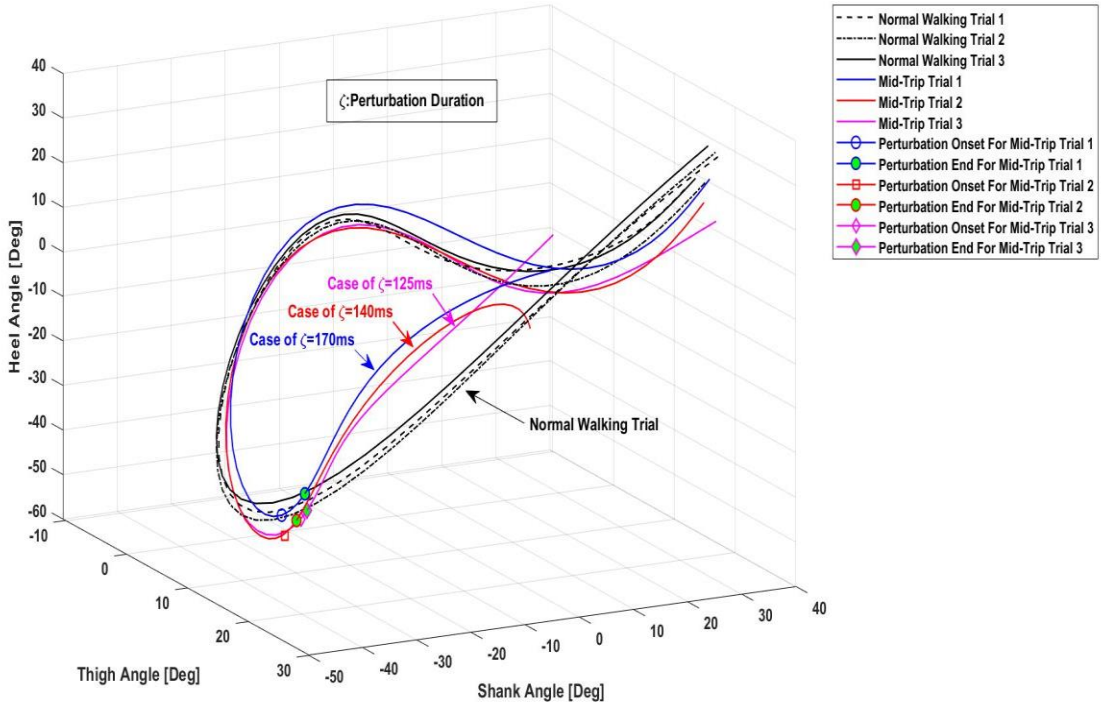

Note. Normal walking curves (blacks) lay in a plan with respect to the PCL law, while for different mid trip cases (bleu, magenta and red) the law is violated and the resultant curves lay with an angle that increases with perturbation duration with respect to the main plan

it can be seen from the previous figure as discussed above that when the trip perturbation gets longer the angles of the results curve with respect to the PCL law gets bigger as well, and to see the response for late trip perturbation type, normal walking and different late trips with different perturbation times durations are presented in Figure 42.

Figure 42

Coplanar Variation Law of Elevating Angles of Thigh, Shank and Thigh During Normal Walking and Late Trip Events with Different Perturbation Lengths

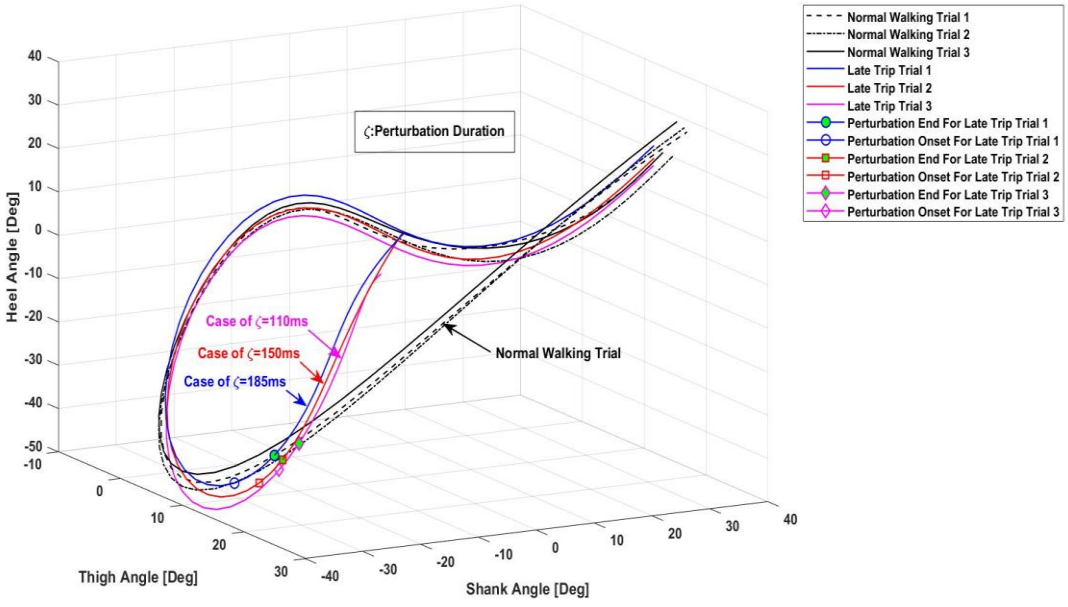

Note. Normal walking curves (blacks) lay in a plan with respect to the PCL law, while for different late trip cases (bleu, magenta and red) the law is violated and the resultant curves lay with an angle that increases with perturbation duration with respect to the main plan.

In order to find a relation between the angle formed by the loop pattern resulted from the correlation of different lower limbs segments elevation angles with respect to the normal walking PCL plane and trip perturbation duration, loop pattern angles are calculated for the entire pattern with respect to the normal walking PCL plan and the maximum deviation angle due to the trip perturbation formed by the trend and the normal walking plane were plotted for thirty trials with respect to perturbation duration and results are shown in Figure 43.

Figure 43

Angle Between Trip Perturbation Plane and Normal Walking PCL Plane as Function of Trip Perturbation Duration

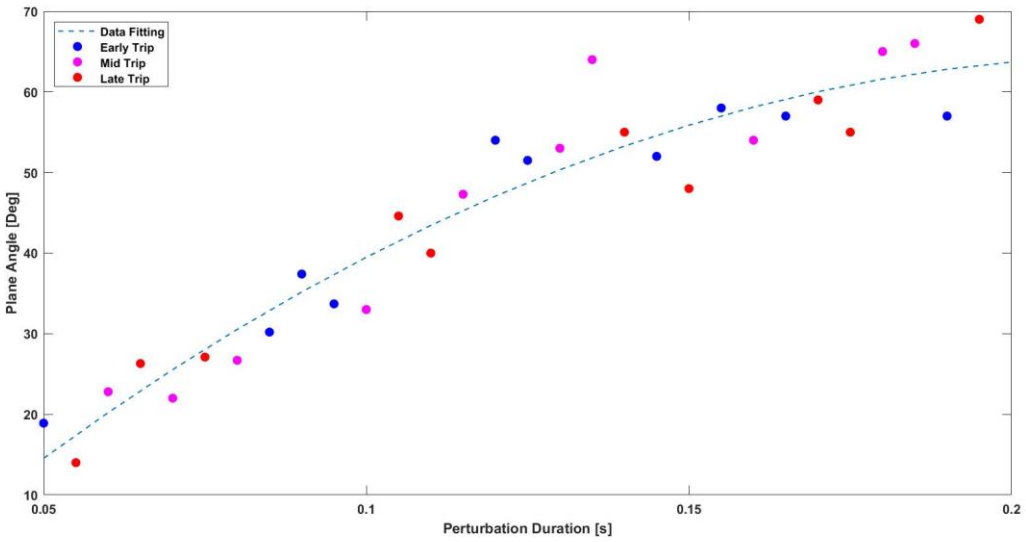

Note. The angle between the trip perturbation plan and the normal walking plane following PCL follow a quadratic pattern as function of trip perturbation duration with 95% confidence bounds fitting curve (dashed blue line)

The equation of the fitting curve as function of the perturbation duration can be expressed as

$$\alpha = -0.0017\zeta^2 + 0.7554\,\zeta - 18.95 \quad (19)$$

With α being the angle between the tripping perturbation plan and normal walking PCL plane and ζ being the trip perturbation duration.

It can be seen that the angle formed between the plane containing the trip perturbation event and the normal walking plane falling under the PCL rule have a quadratic relationship with the perturbation duration , in a sense the long the perturbation duration is , the higher is the formed angle between both planes and the harder is to recover from the trip since such long perturbation will lead to high body center of mass shifting forward that will lead to fall eventually.

Chapter 5

Conclusions and Future Work

In this thesis, time and frequency domain algorithms for rapid trip detection during normal walking are presented. All developed algorithms can detect trip in less than 100 ms, which is faster than the human voluntary reactions (~200 ms). The algorithms use measurements of human lower limb and trunk kinematics as inputs, which were acquired using seven 6 DOF wearable inertial measurement units (IMUs) during human subject experiments. The linear accelerations and angular velocities measurements provided by the IMUs were used to compute the angular displacements, velocities, accelerations and jerks used as the kinematic variables in the algorithms. The proposed algorithms include three static threshold-based detection methods that rely on detecting deviations in human kinematic variables, including the motion of the trunk and lower limb during trip events to detect trip perturbation.

The first algorithm was developed based on the angular jerk (J) of the lower back in the sagittal plane as the main trip indicator. The angular jerk (J) is obtained by integrating numerically the angular velocity measurements from a single IMU mounted at the lower back and the algorithm was able to detect perturbation with mean trip detection time of 43 ms. The second algorithm was designed based on the computed quadratic mean (i.e., root mean square (RMS)) of the angular acceleration signal of the lower back using a sliding window technique with a width of 100 ms. The proposed algorithm showed a trip detection rate of 100% with a mean trip detection time of 51 ms.

The third algorithm uses a statistical measure of the magnitude of the lower back angular acceleration also known as signal magnitude area (SMA) in order to detect changes in the mean signal values when perturbation is induced. The algorithm had a true detection rate of 100% with a mean trip detection time of 66.4 ms.

An optimized elastic time-series alignment tool called dynamic time warping (DTW) that allows the measurement of similarities between two temporal sequences and provides an optimal alignment between both of them was used in order to detect trip perturbation efficiently with a mean trip detection time of 70 ms. Finally, an optimized signal-frequency decomposition method known as continuous wavelet transform (CWT) was used for trip detection that allows signal comparison and analysis in the frequency-time domain to increase robustness of trip perturbation onset detection. The CWT uses a predefined mother wavelet signal that was custom designed based on the average signal of multiple trip events trials. CWT showed a promising result with 100% trip detection rate and a mean trip detection time of 71 ms.

In addition, to cover broader spectrum of trip perturbation analysis, a planar covariation law (PCL) based on intersegmental co-ordination kinematic law was introduces to investigate trip gaits. The PCL relates different elevation angles of lower limb segments during locomotion through a planar relationship in 3D angle space. The Analysis of PCL in trip gaits was demonstrated for the first time in order to provide better understanding about the joint angle kinematic relationships during trip perturbation in relations to the trip severity and its correlation with trip perturbation duration.

An empirical relation and law are proposed in order to relate maximum angle deviation of the trip trajectory from the PCL plane in the 3D elevation angle space of the perturbed lower limb with respect to the perturbation duration. This obtained relationships can potentially correlate the lower limb kinematic relationships during trip with the trip severity and can be potentially used in future design of trip recovery strategies or define limits beyond which the recovery is not possible.

Based on the presented results it can be concluded that all algorithms provide a rapid trip detection with a mean trip detection time of only 61 ms across all methods and with 100% detection rate. Selection of a specific method needs careful considerations based on the advantages and disadvantages of the individual method. For the fixed threshold methods, the coding simplicity, fast information processing of the algorithms, and easy implementation makes them and attractive approach to be used for trip detection. However, the limitations of this algorithm start to manifest when locomotion speed or amplitude vary as function of time.

The DTW-based trip detection method showed the advantages of allowing it to discard the effect of time and amplitude variations during the analysis making it a strong candidate when choosing trip detection methods. However, the complexity of the algorithm in addition to the need of a signal reference and the longer information processing time due to dense algorithm can make it challenging to be implemented for real-time applications compared to the fixed threshold methods.

Finally, CWT-based trip detection methods provide a complete time-frequency analysis approach since it can detect anomalies included in trip signal that cannot be detected in the time domain only and is more robust to any signal variation that can hinder the rate of detection in time domain algorithms. Nevertheless, due to the complexity of the algorithm, the need to provide a mother wavelet as a based reference, and increased computational power to perform calculations makes it more computational demanding compared to other methods and would need to be further tested before can be applied for real-time applications. Overall, all developed trip detection algorithms demonstrated fast detection time being 2-3 times faster compared to the human voluntary responses to perturbations.

The rapid trip detection system can be integrated and combined with an assistive device designed to assist with trip balance recovery as there is a sufficient time between trip detection timing and fall for the system to provide an assistance with the trip balance recovery. The developed trip detection system in this thesis in combination with the robotic assistive technologies have the potential to serve as an enabling tools of future trip-and-fall prevention strategies.

5.1. Future Work

There are several future directions of this work. First, the static threshold methods will be optimized and enhanced by creating more dynamic thresholds that can adapt and change with respect to actual locomotion signal variation and thus increase its flexibility and efficiency. For both DTW and CWT methods, a more advanced optimization process of the algorithms will be conducted in order to reduce the amount of dependability on the

fixed reference signals in their trip/no trip decision, which will make them more flexible, and the computational complexity of the algorithm has to be reduced to make it more suitable for real time application implementation.

Another future research direction is the integration of the proposed PCL kinematic law with the presented algorithms in order to make the full system not only able to detect trip but predict its severity based on the measured duration of the perturbation. Such integration will allow assistive system to provide the needed amount of torque based on the information provided by the PCL quantification and the detection algorithm in order to provide an external assistance and prevent falls.

All these algorithms have to be further tested on multi-subject experiments to further confirm its validity across all populations. A long-term goal is to validate the efficacy of this algorithm using assistive trip-and-fall prevention device in laboratory and real-world settings to potentially contribute to the design of advanced fall prevention systems by providing detection of trip perturbations and thus preventing falls.

References

[1] M. J. Pavol, T. M. Owings, K. T. Foley, M. D. Garbiner, "Gait Characteristics as Risk Factors for Falling from Trips Induced in Older Adults", Journal of Gerontology: Medical Sciences, Vol. 54A, No. 11, 1999. (b)

[2] W.P. Berg, H.M. Alessio, E.M. Mills, C. Tong," Circumstances and consequences of falls in independent community-dwelling older adults", Age Ageing, 26 (4) (1997), pp. 261-268

[3] M.J. Heijnen, S. Rietdyk. "Falls in young adults: perceived causes and environmental factors assessed with a daily online survey", Hum. Mov. Sci., 46 (2016), pp. 86-95.

[4] R. McNanmee, K. Kemmlert, L. Lundholm, N. M. Cherry, "Injuries After Falls at Work in the United Kingdom and Sweden with Special Reference to Fractures in Women Over 45.", Journal of Occupational Environment Medicine, Vol. 54, p. 785 –792, 1997.

[5] R. A. Andersen and E. Lagerlöf, "Accident Data in the New Swedish Information System on Occupational Injuries", Ergonomics, Vol. 26, No. 1, p. 33 - 42, 1983

[6] Tinetti ME, Speechley M, Ginter SF. "Risk factors for falls among elderly persons living in the community". N Engl J Med. 1988;319:

[7] L. J. Donaldson, A. Cook, and R. G. Thomson, "Incidence of fractures in a geographically defined population," Journal of epidemiology and Community Health, vol. 44, no. 3, pp. 241-245, 1990.

[8] E. Zaloshnja, T.R. Miller, B.A. Lawrence, E. Romano." The costs of unintentional home injuries", Am. J. Prev. Med., 28 (1) (2005), pp. 88-94. M. J. Pavol, T. M. Owings, K. T. Foley, M. D. Garbiner, "Gait Characteristics as Risk Factors for Falling from Trips Induced in Older Adults", Journal of Gerontology: Medical Sciences, Vol. 54A, No. 11, 1999. (b)

[9] J. C. Davis, D. P. Manning, G. J. Kemp, and S. P. Frostick, "The Rising Number of Underfoot Accidents After the Menopause Causes Both Fractures and Non-Fracture Injuries." Quarterly Journal of Medicine, Vol. 94, p. 699 – 707, 2001.

[10] Health & Safty Comission," Health and Safty Statistics 2000/2001-National Statistics",HSE Book,ISBN 0717621103,2001.

[11] Y.Ocubo ,M.A. Brodie, D.Sturnieks ,C Hikes, H.Carter, "Exposure to Trips and Slips with Increasing Unpredictability while Walking Can Improve Balance Recovery Responses with Minimum Predictive Gait Alterations", 0202913,pp. 230-235,2018.

[12] M.E.Eveld,S.T King,L.G.Vilati,K.E.Ezik," On the Basis for Stumble Recovery Strategy Selection in Healthy Adults",J biomechanical Engineering, doi: 10.1115/1.4050171,2021

[13] M. J. Pavol, T. M. Owings, K. T. Foley, M. D. Garbiner, "Mechanisms Leading to a Fall from an Induced Trip in Healthy Older Adults", Journal of Gerontology: Medical Sciences, Vol. 56A, No. 7, p. M428 – M437, 2001.

[14] T. M. Owings, M. J. Pavol, M. D. Grabiner, "Mechanisms of Failed Recovery Following Postural Perturbations on a Motorised Treadmill Mimic those Associated with an Actual Forward Trip", Clinical Biomechanics, Vol. 16, p. 813 – 819, 2001.

[15] A. J. van der Bogert, M. J. Pavol, M. D. Grabiner, "Response Time is More Important than Walking Speed for the Ability of Older Adults to Avoid a Fall After a Trip", Journal of Biomechanics, Vol, 35, p. 199 – 205, 2002.

[16] C.Shirota, A.M. Simon, T.A.Kuiken," Trip recovery strategies following perturbations of variable duration", Journal of Biomechanics (47)2679-2684,2014.

[17] M. C. Nevitt, S. R. Cummings, S. Kidd, D. Black, "Risk Factors for Recurrent Nonsyncopal Falls: A Prospective Study", Journal of the American Medical Association, Vol. 261, p. 2663 – 2668, 1989.

[18] M. J. Pavol, T. M. Owings, K. T. Foley, M. D. Garbiner, "Gait Characteristics as Risk Factors for Falling from Trips Induced in Older Adults", Journal of Gerontology: Medical Sciences, Vol. 54A, No. 11, p. M583 – M590, 1999.

[19] A. J. van der Bogert, M. J. Pavol, M. D. Grabiner, “Response Time is More Important than Walking Speed for the Ability of Older Adults to Avoid a Fall After a Trip”, Journal of Biomechanics, Vol, 35, p. 199 – 205, 2002.

[20] M.L. Morry, S. Jeffries,” Trip Feasibility Study Report Number HSL/2006/77”, Human Factors Group, 2003.

[21] Y. C. Smeesters, W. C. Hayes, T. H. McMahon, “Disturbance Type and Gait Speed Affect Fall Direction and Impact Location”, Journal of Biomechanics, Vol. 34, p. 309– 317, 2001.

[22] K. Thella,et all, ‘‘Smart unit care for pre fall detection and prevention,’’ in Proc. IEEE Nat. Aerosp. Electron. Conf. (NAECON), Jul. 2016,

[23] Hu X, Qu X. “An individual-specific fall detection model based on the statistical process control chart”. Saf Sci. 2014; 64:13–21.

[24] Zhao G, Mei Z, Liang D, Ivanov K, Guo Y, Wang Y, Wang L. “Exploration and implementation of a pre-impact fall recognition method based on an inertial body sensor network”. Sensors (Basel). 2012; 12:15338–55.

[25] Liu J, Lockhart TE. “Development and evaluation of a prior-to-impact fall event detection algorithm”. IEEE Trans Biomed Eng. 2014; 61:2135–40

[26] Young retail workers, Prevent Slips, Trips, and Falls, Center for disease control and prevention CDC, The national institute for occupational safety and health NIOSH ,2018

[27] Zitouni, M., Pan, Q., Brulin, D., and Campo, E.” Design of a smart sole with advanced fall detection algorithm”,J. Sensor Technol. 9:71. doi: 10.4236/jst.2019.94007

[28] Putra, I., Brusey, J., Gaura, E., and Vesilo, R.”An event-triggered machine learning approach for accelerometer-based fall detection”. Sensors 18, 20. doi: 10.3390/s18010020,2017

[29] Thilo, F. J., Hahn, S., Halfens, R. J., and Schols, J.M. “Usability of a wearable fall detection prototype from the perspective of older people-a real field-testing approach”. J. Clin. Nurs. 28, 310–320. doi: 10.1111/jocn.14599,2019

[30] Xi, X., Tang, M., Miran, S. M., and Luo, Z. (2017). “Evaluation of feature extraction and recognition for activity monitoring and fall detection based on wearable SEMG sensors”. Sensors 17, 1229. doi: 10.3390/s17061229

[31] G.Mizzini,F.Apregiliano,V.Monaco,D.D.Ventura,”EEG/EMG based Architecture for the Early Detection of Slip-induced Lack of Balance”, IEEE 8th International Workshop on Advances in Sensors and Interfaces,18936055,2019

[32] S.Hashemi, A., Nasiopoulos, P., Little, J. J., and Pourazad, M. T..“Video-based human fall detection in smart homes using deep learning,” ,IEEE International Symposium on Circuits and Systems (ISCAS) (Florence:IEEE), 1–5. doi: 10.1109/ISCAS.2018.8351648,2018

[33] Akagündüz, E., Aslan,M., ¸Sengür, A.,Wang, H., and˙Ince,M. C. “Silhouette orientation volumes for efficient fall detection in depth videos”. IEEE J. Biomed.Health Inform. 21, 756–763. doi: 10.1109/JBHI.2016.2570300,2017

[34] Mastorakis, G., and Makris, D.”Fall detection system using kinect’s infrared sensor”. J. Realtime Image Process. 9, 635–646. doi: 10.1007/s11554-012-0246-9,2014

[35] Charfi, I., Miteran, J., Dubois, J., Atri, M., and Tourki, R. “Definition and performance evaluation of a robust SVM based fall detection solution”. SITIS 12, 218–224. doi: 10.1109/SITIS.2012.155,2012

[36] Cai, Z., Han, J., Liu, L., and Shao, L.” RGB-D datasets using Microsoft Kinect or similar sensors: a survey. Multimedia Tools Appl”. 76, 4313–4355. doi: 10.1007/s11042-016-3374-6

[37] Martínez-Villaseñor, L., Ponce, H., Brieva, J., Moya-Albor, E., Núñez-Martínez, J., and Peñafort-Asturiano, C. “Up-fall detection dataset: a multimodal approach”. Sensors 19:1988. doi: 10.3390/s19091988,2019

[38] Ma, C., Shimada, A., Uchiyama, H., Nagahara, H., and Taniguchi, R.-i. “Fall detection using optical level anonymous image sensing system”. Optics Laser Technol. 110, 44–61. doi:10.1016/j.optlastec.2018.07.013

[39] Liu, L., Popescu,M., Skubic,M., and Rantz,M.. “An automatic fall detection framework using data fusion of Doppler radar and motion sensor network,”, 36th Annual International Conference of the IEEE Engineering inMedicine and Biology Society (Chicago, IL: IEEE), 5940–5943.,2014

[40] Yazar, A., Erden, F., and Cetin, A. E. “Multi-sensor ambient assisted living system for fall detection,” in Proceedings of the IEEE International Conference on Acoustics, Speech, and Signal Processing (ICASSP-14) (Florence), 1–3,2014

[41] X.Hu,X,Qu,”Pre-impact fall detection”,Biomedical Engineering J OnLine, DOI 10.1186/s12938-016-0194-x,2016

[42] K. Thella,et all, ‘‘Smart unit care for pre fall detection and prevention,’’ in Proc. IEEE Nat. Aerosp. Electron. Conf. (NAECON), Jul. 2016,

[43] Wu G. “Distinguishing fall activities from normal activities by velocity characteristics”. J Biomech.;33:1497–500,2000

[44] Aziz O, Russell CM, Park EJ, Member S, Robinovitch SN. “The effect of window size and lead time on pre-impact fall detection accuracy using support vector machine analysis of waist mounted inertial sensor data”. IEEE engineering in medicine and biology society.,2014.

[45] Lee JK, Robinovitch SN, Park EJ, Member S. “Inertial sensing-based pre-impact detection of falls involving near-fall scenarios”. IEEE Trans Neural Syst Rehabil Eng.; 23:258–66.,2015

[46] Aprigliano, F. et. al., “Pre-Impact Detection Algorithm to Identify Tripping Events Using Wearable Sensors”, Sensors, 19.17 (2019): 3713.

[47] Sucerquia, A., López, J., and Vargas-Bonilla, J. (2018). “Real-life/real-time elderly fall detection with a triaxial accelerometer”. Sensors 18:1101. doi: 10.3390/s18041101

[48] Salleh, S.M.; mohd yusoff, a.h.; ngadimon, K.; Koh, C.Z. “Neural Network Algorithm-based Fall Detection Modelling”. Int. J. Integr. Eng. 2020, 12, 138–150.

[49] Kumar, V.C.; Ha, S.; Sawicki, G.; Liu, C.K. “Learning a Control Policy for Fall Prevention on an Assistive Walking Device”. IEEE International Conference on Robotics and Automation (ICRA), August 2020; pp. 4833–4840.

[50] Mauldin, T.R.; Canby, M.E.; Metsis, V.; Ngu, A.H.; Rivera, C.C. SmartFall: “A smartwatch-based fall detection system using deep earning”. Sensors 2018, 18, 3363. [CrossRef] [PubMed]

[51] Chen, K.-H., Hsu, Y.-W., Yang, J.-J., and Jaw, F.-S. (2017b). “Enhanced characterization of an accelerometer-based fall detection algorithm using a repository”. Instrument. Sci. Technol. 45, 382–391. doi: 10.1080/10739149.2016.1268155

[52] Drover, D.; Howcroft, J.; Kofman, J.. “Faller classification in older adults using wearable sensors based on turn and straight-walking accelerometer-based features”. Sensors 2017, 17, 1321.

[53] Putra, I.; Brusey, J.; Gaura, E.; Vesilo, R. “An event-triggered machine learning approach for accelerometer-based fall detection”. Sensors 2018, 18, 20. [CrossRef]

[54] Nait Aicha, A.; Englebienne, G.; Van Schooten, K.S.; Pijnappels, M.; Kröse, B. “Deep learning to predict falls in older adults based on daily-life trunk accelerometry”. Sensors 2018, 18, 1654. [CrossRef]

[55] Islam, Z. Z., Tazwar, S. M., Islam, M. Z., Serikawa, S., and Ahad, M. A. R. “Automatic fall detection system of unsupervised elderly people using smartphone,” in 5th IIAE International Conference on Intelligent Systems and Image Processing 2017 (Hawaii), 5. doi: 10.12792/icisip2017.077

[56] Saleh, M., and Jeannés, R. L. B. (2019). “Elderly fall detection using wearable sensors: a low cost highly accurate algorithm”. IEEE Sens. J. 19, 3156–3164. doi: 10.1109/JSEN.2019.2891128

[57] Zitouni, M., Pan, Q., Brulin, D., and Campo, E. (2019). “Design of a smart sole with advanced fall detection algorithm”. J. Sensor Technol. 9: 71.doi: 10.4236/jst.2019.94007

[58] Wu, T., Gu, Y., Chen, Y., Xiao, Y., and Wang, J. (2019). “A mobile cloud collaboration fall detection system based on ensemble learning”. arXiv [Preprint]. arXiv:1907.04788.

[59] Xi, X., Tang, M., Miran, S. M., and Luo, Z. (2017). “Evaluation of feature extraction and recognition for activity monitoring and fall detection based on wearable SEMG sensors”. Sensors 17, 1229. doi: 10.3390/s17061229.

[60] D. Razum, G. Seketa, J. Vugrin, and I. Lackovic, `”Optimal threshold selection for threshold-based fall detection algorithms with multiple features", in Proc. 41st Int. Conv. Inf. Commun. Technol., Electron. Micro-electron. (MIPRO), Opatija, Croatia, May 2018, pp. 1513-1516.

[61] N. P. Pham, H. V. Dao, H. N. Phung, H. Van Ta, N. H. Nguyen, and T. T. Hoang, “Classification different types of fall for reducing false alarm using single accelerometer," in Proc. IEEE 7th Int. Conf. Commun. Electron. (ICCE), Hue, Vietnam, Jul. 2018, pp. 316-321.

[62] Q. Zhang, L. Ren, and W. Shi, ``HONEY: A multimodality fall detection and telecare system," Telemed. E Health, vol. 19, no. 5, pp. 415-429, May 2013.

[63] F. Zhao, Z. Cao, Y. Xiao, J. Mao, and J. Yuan, “Real-time detection of fall from bed using a single depth camera”, IEEE Trans. Autom. Sci. Eng., to be published. doi: 10.1109/TASE.2018.2861382.

[64] L. Ren, W. Shi, Z. Yu, and Z. Liu,”Real-time energy-efficient fall detection based on SSR energy efficiency strategy”, Int. J. Sensors Netw., vol. 20, no. 4, pp. 243-251, 2016.

[65] W. Min, H. Cui, H. Rao, Z. Li, and L. Yao, “Detection of human falls on furniture using scene analysis based on deep learning and activity characteristics”, IEEE Access, vol. 6, pp. 9324pp9335, 2018.

[66] C.Shirota et all, “Trip recovery strategies following perturbations of variable duration”, 2014

[67] C.Shirota et all,“The effect of perturbation onset timing and length on tripping recovery strategies” ,2011

[68] B. Sharafi et all,” Evidence of impaired neuromuscular responses in the support leg to a destabilizing swing phase perturbation in hemiparetic gait”, 2015

[69] Y. Wang, S. Wang, T. Kaur,R. Bolton,T,Bhat,” Effects of task-specific obstacle-induced trip-perturbation training: proactive and reactive adaptation to reduce fall-risk in community-dwelling older adults”, Aging Clinical and Experimental Research,doi /10.1007/s40520-019-01268-6, July 2019.

[70] M.Joshi,P.Patel,T.Bhatt,” Reactive balance to unanticipated trip-like perturbations: a treadmill-based study examining effect of aging and stroke on fall risk”,J International Biomechanics, doi10.1080/23335432.2018.1512375,2018

[71] E. Maura, T.K., Shane, L.G.Vailati , K.E,Zelik , M. Goldfarb,” On the Basis for Stumble Recovery Strategy Selection in Healthy Adults”, Journal of biomechanical engineering, 2021-07-01, Vol.143 (7)

[72] D.A.Winter, ”Biomechanics and Motor Control of Human Movement”, Fourth Edition, John Wiley & Sons, Inc. ISBN: 978-0-470-39818-0,2009

[73] K. Racz, R.M. Kiss,” Marker displacement data filtering in gait analysis: A technical note”, J,Biomedical Signal Processing and Control, doi 10.1016/j.bspc.2021.102974,2021

[74] T. M. Owings, M. J. Pavol, M. D. Grabiner, “Mechanisms of Failed Recovery Following Postural Perturbations on a Motorised Treadmill Mimic those Associated with an Actual Forward Trip”, Clinical Biomechanics, Vol. 16, p. 813 – 819, 2001.

[75] C.Shirota,A.M. Simon,T.A.Kuiken,” Trip recovery strategies following perturbations of variable duration”,Journal of biomechanics, doi jjbiomech.2014.05.009,2014

[76] Farzin Dadashi, et all, “Gait and Foot Clearance Parameters Obtained Using Shoe-Worn Inertial Sensors in a Large-Population Sample of Older Adults” ,2014

[77] D.S.Marigold, J.E.Misiaszeck,” Whole-Body Responses: Neural Control and Implications for Rehabilitation and Fall Prevention”, Sage Journal,The neuroscientist doi 10.1177/1073858408322674,2008

[78] H. Hyati,D.Eager,A.M.Pendrill,H.Alberg,”Jerk within the Context of Science and Engineering—A Systematic Review”,Vibration Journal,doi 10.3390/vibration3040025,pp 371-409,2020.

[79] Mathie MJ, Coster AC, Lovell NH, Celler BG. “Detection of daily physical activities using a triaxial accelerometer”. Med Biol Eng Comput.;41(3):296–301. doi/10.1007/BF02348434,2003.

[80] Curone D, Bertolotti GM, Cristiani A, Secco EL, Magenes G. “A real-time and self-calibrating algorithm based on triaxial accelerometer signals for the detection of human posture and activity”. IEEE Trans Inf Technol Biomed.; 14(4):1098–1105,2010

[81] M. T. Redfield, J. C. Cagle,; B. J. Hafner; J. E. Sanders, ,”Classifying prosthetic use via accelerometry in persons with transtibial amputations” , MSEE ,Volume 50 Number 9, 2013

[82] M.Sekine,T.Tamuro,Y.Suda,Y.Kimura,Y.Kijima,Y.Higashi,T.Fijumoto ,” A gait abnormality measure based on root mean square of trunk acceleration”, Journal of NeuroEngineering and Rehabilitation, pp 233-234,2013

[83] Cartwright, Kenneth V . "Determining the Effective or RMS Voltage of Various Waveforms without Calculus" (PDF). Technology Interface. 8 (1): 20 pages.

[84] Yurika Permanasari et al,” Speech recognition using Dynamic Time Warping (DTW)”, J. Phys.: Conf. Ser. 1366 012091,2019

[85] Brijnesh J. Jain , David Schultz,” Optimal Warping Paths are unique for almost every Pair of Time Series”, Statistical pattern recognition in non-Euclidean spaces J, Technische Universit¨at Berlin, Germany,2018

[86] E.Antonsson et al.,”The frequency content of gait”, Journal of biomechanics. , 1985, Vol.18(1), p.39-47

[87] N.A.Borghese,S.Lucia,”Kinematic determinates of human locomotion”,Journal of phisyologie, 494.3, pp.863-879,1996

[88] F.Aprigiliano,V.Monaco,S.Micera,” External sensory-motor cues while managing unexpected slippages can violate the planar covariation law”,Journal of biomechanics,2019